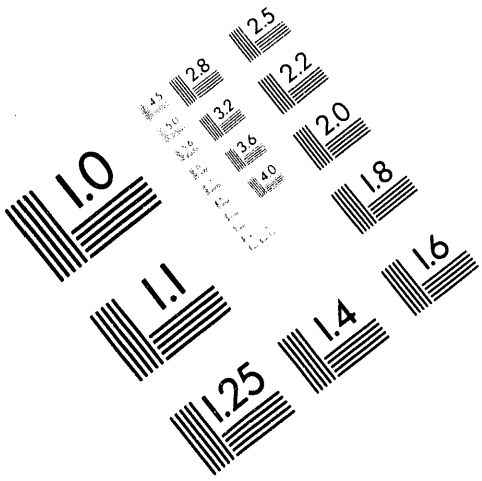

Association for Information and Image Management

1100 Wayne Avenue, Suite 1100
Silver Spring, Maryland 20910

301/587-8202

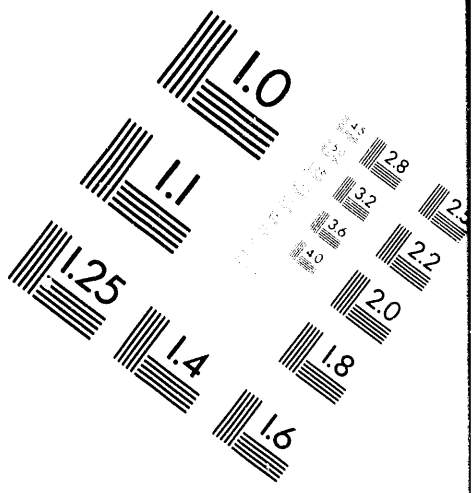

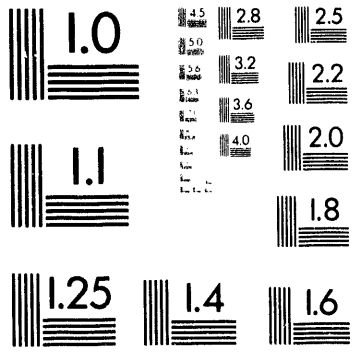

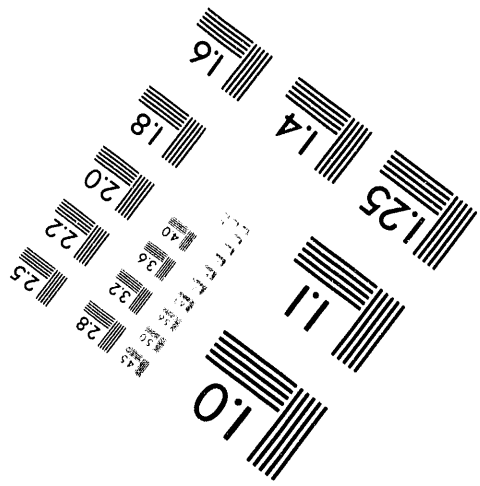

MANUFACTURED TO AIIM STANDARDS
BY APPLIED IMAGE, INC.

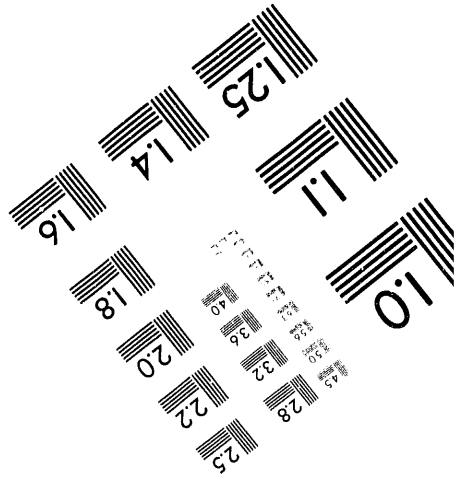

1 of 1

10/5/31-94(98&1)

SANDIA REPORT

SAND94-8219B • UC-704
Unlimited Release
Printed May 1994

Supersedes SAND94-8219, Printed February 1994

Compilation of Diamond-Like Carbon Properties for Barriers and Hard Coatings

D. A. Outka, W. L. Hsu, K. Phillips, D. R. Boehme,
N. Y. C. Yang, D. K. Ottesen, H. A. Johnsen,
T. J. Headley, W. M. Clift

Prepared by
Sandia National Laboratories
Albuquerque, New Mexico 87185 and Livermore, California 94551
for the United States Department of Energy
under Contract DE-AC04-94AL85000

SAND94-8219B
Unlimited Release
Printed May 1994

UC-404

Supersedes SAND94-8219, Printed February 1994

COMPILATION OF DIAMOND-LIKE CARBON PROPERTIES FOR BARRIERS AND HARD COATINGS

Duane A. Outka, Wen L. Hsu, K. Phillips,
Dale R. Boehme, Nancy Y. C. Yang, Dave K. Ottesen,
Howard A. Johnsen, W. Miles Clift
Sandia National Laboratories/California

and

Thomas J. Headley
Sandia National Laboratories/Albuquerque

ABSTRACT

Diamond-like carbon (DLC) is an amorphous form of carbon which resembles diamond in its hardness, lubricity, and resistance to chemical attack. Such properties make DLC of interest for use in barrier and hard coating technology. This report examines a variety of properties of DLC coatings which are relevant to its use as a protective coating. This includes examining substrates on which DLC coatings can be deposited; the resistance of DLC coatings to various chemical agents; adhesion of DLC coatings; and characterization of DLC coatings by electron microscopy, FTIR, sputter depth profiling, stress measurements, and nanoindentation.

TABLE OF CONTENTS

Page

1.0 Introduction – Wen Hsu 9

2.0 Deposition Rate versus Process Parameters - Kristen Phillips and Duane Outka 10

3.0 DLC-Substrate Compatibility - Duane Outka 13

4.0 Chemical Resistance of DLC Coatings - Dale Boehme 14

5.0 Electron Microscope Analysis of DLC Coatings - Nancy Yang, Thomas J. Headley, and Miles Clift 18
- 5.1 HRTEM Study of DLC 18
- 5.2 Analysis of Adhesion Failure of DLC to Iron using SEM 19
- 5.3 Analysis of Adhesion of DLC to 303 Se Stainless Steel using SEM 22

6.0 FTIR Studies of DLC Coatings - Dave Ottesen and Howard Johnsen 26

7.0 Stress in DLC Films - Duane Outka and Kristen Phillips 29
- 7.1 Sources of Stress in DLC Films 29
- 7.2 Previous Studies of DLC Film Stress 30
- 7.3 Measurements of Stress in DLC Films 32

8.0 Adhesion of DLC Coatings - Duane Outka 35
- 8.1 Mechanical and Chemical Properties of Diamond Relevant to Adhesion 35
- 8.2 Previous Studies of DLC Film Adhesion 39
- 8.3 Strategies to Improve Adhesion of DLC Coatings 41
- 8.4 Chemical Issues for Interlayers Used to Improve the Adhesion of Carbon Films on Iron Substrates 43

9.0 Hardness Testing - Duane Outka and Wen Hsu 47

10.0 Conclusions - Wen Hsu 47

11.0 Acknowledgments 48

12.0 References 49

ILLUSTRATIONS

No.		Page
2.1	The Effect of RF Power and Methane Pressure on Deposition Rate	12
2.2	DLC Depth versus Deposition Time	12
3.1	Structural Formulas for Selected Compounds Listed in Table 3.1	13
4.1	Diagram Representing Chemical Test Procedure	15
4.2	Micrograph Showing Area of DLC Coating Exposed to HCl	15
4.3	Individual Defect Produced by Reaction of HCl and Al Substrate Showing Delamination of the Coating as HCl/substrate Reaction Progresses	16
4.4	SEM Micrograph Showing Stress Cracking and Pin-hole Formation	16
4.5	Optical Micrograph Showing Inclusions Exposed on the Surface of an Al-6061-T6 Polished Disk	17
4.6	Micrograph of Al-6061-T6 Polished Disk with DLC Coating with a Silicon Interlayer—After Exposure to Concentrated HCl	18
5.1.1	HRTEM Showing Amorphous Nature of DLC	20
5.1.2	DLC with some Impurities that Contain Crystallinity	20
5.2.1	Optical Image Showing Regions of Coating Failure	21
5.2.2	Optical Image Shows that the Failure Proceed along the Direction of the Grooves	21
5.2.3	Typical Image Shows of Discolored Area	23
5.3.1	(a) Optical Micrograph Showing DLC Flakes Peeling off the Substrate (130x) (b) SEM Micrograph Showing Loose DLC Flakes (100x)	23
5.3.2	(a) Typical Bent Flakes; (b) No Carbon was Detected on the Concave Side Indicating it is from the Si-stainless Steel Interface. (c) Carbon was Detected on the Convex Side Indicating it is the DLC Surface	25
5.3.3	AES Depth Profile of Failed DLC Coating on 303 Se Stainless Steel Showing Oxygen Impurity at Fe-C Interface	25
6.1	FTIR Spectra of a 0.4 μm Thick DLC Film on Si(100) Heated to Various Temperatures up to 550° C	27

No.		Page
6.2	FTIR Spectra of a 1.0 μm Thick DLC Film on Si(100) Heated to Various Temperatures up to 550° C	27
6.3	FTIR Spectra of a 2.1 μm Thick DLC Film on Si(100) Heated to Various Temperatures up to 550° C	28
7.1	Schematic of Stress Measuring Apparatus	33
7.2	DLC Coating Thickness Versus Deposition Time	34
7.3	Stress Versus Coating Thickness for DLC on Aluminum Substrates	34

TABLES

No.		Page
3.1	List of DLC Compatible Substrates	13
3.2	List of DLC Incompatible Substrates	14
7.1	Mechanical and Thermal Properties of Materials	30
7.2	Quantitative Stress Measurements for DLC and Diamond Films	31
7.3	Measurements of Stress in DLC Coatings Prepared at Sandia	34
8.1	Carbon Bond Dissociation Energies	37
8.2	Thermodynamic Properties of Carbides	38
8.3	Elements with Stable and Unstable Carbides	39
8.4	Quantitative Adhesion Measurements for DLC and Diamond Films	40
8.5	Binary Alloys and Compounds of Iron [62]	44
8.6	Thermodynamic Properties of Binary Iron Compounds and Alloys	44
8.7	Thermodynamic Properties of Binary Ion Compounds and Alloys at Elevated Temperature	45

COMPILATION OF DIAMOND-LIKE CARBON PROPERTIES FOR BARRIERS AND HARD COATINGS

1.0 Introduction – Wen Hsu

Carbon as a solid material can exist in several phases including graphite, diamond, and fullerenes. These materials have definite atomic structures with a long range order. Carbon materials, however, can also be processed to have a much shorter range of atomic order; if the processing conditions are chosen properly one can obtain a purely amorphous phase. Among such, diamond-like carbon (DLC) is a term used to describe all amorphous carbon that has a high degree of sp^3 (or tetrahedral) bonding.

Diamond-like carbon films have been studied for more than two decades. The first report of DLC films was by Aisenberg and Chabot [1], followed by a series of reports by Holland [2, 3] and Weissmantel [4, 5]. A more recent paper that gives a comprehensive review of the subject is by Angus, Koidl, and Domitz [6].

Interest in DLC is primarily fueled by its unusual properties and potential promise in several applications. These films are relatively resistant to chemical attack, have a high hardness, and have good optical transparency. Furthermore, they can be deposited at relatively low temperatures and are, therefore, compatible with a wide variety of materials.

Several techniques have been reported to successfully deposit DLC films. Typically methane is chosen as the carbon bearing gas. Since high bombarding energies (> 100 eV) are necessary to produce films with a high degree of sp^3 bonding, the working pressure is typically < 100 mTorr. To accelerate the carbon atoms, the hydrocarbon gas molecules are ionized either in an ion source and then extracted by accelerating grids, or in a plasma discharge and then bombarded onto the growth surface by the high potential difference that is formed in the discharge sheath. Many variants on these two basic concepts exist. For example, a commercial process that is used by Diamonex relies on depositing carbon from a sputtered graphite target and then bombarding the carbon collecting surface by an argon ion source. Depending upon the carbon source used, the deposited films can have a hydrogen content ranging from 0 atomic percent up to 40 atomic percent. For example, the Diamonex process produces films that are are nearly hydrogen free. In our case, we rely on discharges in a methane gas, and the films have hydrogen up to 40 atomic percent.

In our work we decided to employ a plasma-based deposition process [7] for two reasons. First, we can choose from a variety of gas sources that contain other elemental species, such a silicon, metal, and halogens which provides a degree of freedom to tune the properties of the films. Second, the plasma can be made to "wrap" around the deposition surface to conform to the shape of the coated surface. This is distinct from the line-of-sight deposition in other processing methods and offers an advantage when the coated substrates have contoured shapes.

The plasma discharge is formed between an electrode and the grounded vacuum vessel. The electrode serves as the surface where coating is to be deposited, and radio-frequency power (13.56 MHz) is applied through a coaxial cable to the electrode. For example, if a contoured metal plate must be coated, the powered central lead of the coaxial-cable is connected to the electrode and the outer grounded shield is connected to the vacuum vessel. The electrode-vacuum vessel geometry essentially resembles a capacitor where RF is applied between the two ends of the capacitor. The electric field at the electrode end of the capacitor has a higher intensity, because the surface area of the electrode is typically smaller, or at best comparable to the surface area of the vacuum vessel. When a discharge is initiated, the plasma will be concentrated around the electrode surface, giving rise to the discharge conformality.

The high acceleration voltage that exists at the plasma-electrode sheath (typically reaching up to several hundred eV) is a plasma physics phenomenon. The mobility of electrons is much higher (mobility scales as the inverse square root of the mass), because of the significantly lower mass of electrons compared to ions. Since the plasma must be electrically neutral on a macroscopic scale, every electron that is lost to the electrode must be balanced by an equal loss of ions, when averaged over time (over several periods of the RF cycle). Since the electron mobility is much higher, the loss of ions to the electrode cannot keep up with that for electrons over long periods of time. The two losses can be balanced provided that the plasma as a whole charges up positively relative to the electrode potential such that on the average electrons are repelled and ions accelerated. The carbon ions, however, do not impinge the surface at the full voltage of the "DC self-bias". The plasma sheath has a finite spatial extent. At a plasma density of ~10^9 cm^{-3}, the sheath thickness is on the order of ~ 1cm. Depending on the gas pressure, this thickness can become comparable to the mean-free-path of collision with gas molecules which would lower the energy of the carbon ions. Therefore, in order to achieve the full benefit of the accelerating voltage, the discharge is typically operated at <100 mTorr. The low pressure limit is determined by the requirement to maintain a discharge. At too low a pressure, an electron in the plasma is not able to create another free electron through ionization before being lost to the electrode, with the result that the plasma cannot be maintained.

In this work we work only with methane as the feed gas, although other hydrocarbon species can also be used. The primary discharge parameters we use to optimize the film properties are discharge power and gas pressure. The substrate is cooled by blowing air against the back face of the electrode. The substrate temperature is crudely estimated to be ≤ 100 °C because the sample is not too hot to be handled after venting the reactor.

2.0 Deposition Rate versus Process Parameters - Kristen Phillips and Duane Outka

During 1993, a new PECVD (plasma-enhanced chemical vapor deposition) reactor was constructed at Sandia with the capability of depositing DLC coatings. This reactor was a significant enhancement over the original reactor (commonly called LAMPE), because it included (1) safety controls so that silane could be used as a source gas to deposit silicon which is used to improve the adhesion of DLC to ferrous substrates (see section 8.4); (2) greater control over pumping

speed so that a wider range of process pressures could be achieved; and (3) a larger 3 inch diameter substrate holder.

In the new reactor, a study was performed to measure the deposition rate as a function of the two major process variables: methane pressure and RF power. The results are based upon approximately a dozen different depositions of DLC onto Si(111) wafers. The amount of DLC deposited was measured both profilometry and by weight change.

Fig. 2.1 illustrates the effect of RF power on the deposition rate and indicates that at low RF power, the deposition rate depends approximately linearly upon RF power. For example, the deposition rate increased by approximately a factor of 2 upon increasing the RF power from 40 to 80 Watts for the two methane pressures used in these measurements. Note also, that the deposition rate could be extrapolated backwards to the origin of the plots in **Fig. 2.1.** At higher RF powers, however, the deposition rate reaches a plateau. For example, there was only a modest increase in deposition rate upon increasing the RF power from 80 to 160 Watts with a constant 68 mTorr pressure. This plateau in deposition rate is attributed to entering a regime where the deposition rate is limited by the methane pressure. It was decided not to operate at 160 Watts, however, after the RF cable between the tuner and the electrode failed during one of the runs at this power. Routine DLC depositions were conduced at 80 Watts of RF power which maximized the deposition rate without leading to equipment breakdowns.

Fig. 2.1 also illustrates the effect of methane pressure on the deposition rate. Again, a higher deposition rate was observed at the higher methane pressures. The highest pressure that is currently attainable in the PECVD reactor is approximately 68 mTorr. This is limited by the conductance of the iris valve between the chamber and the turbomolecular pump. That is, the iris valve cannot be closed further to reduce the pumping speed and thus increase the methane pressure. It is also undesirable to operate at higher methane pressure, because gas-phase collisions will lower the energy of the energetic particles responsible for DLC deposition and lead to a lower quality DLC coating. Based upon these results, routine DLC depositions were conducted at 68 mTorr methane pressure.

Several DLC depositions were performed under the chosen conditions of 80 Watts RF power and 68 mTorr to verify that the deposition rate was linear with deposition time. This also enabled us to determine the deposition time required to deposit films of particular thicknesses of interest such as 0.1 and 1.0 μm. **Fig. 2.2** shows the depth of the DLC coating as a function of deposition time. The deposition rate was reasonably linear with a rate of 6 Å per second. There was a slight offset from the origin of approximately 2 minutes which is attributed to time required to nucleate the coating. The dotted horizontal lines show the target depths of 0.1 and 1.0 μm which are achievable with deposition times of 4.5 and 28 minutes, respectively.

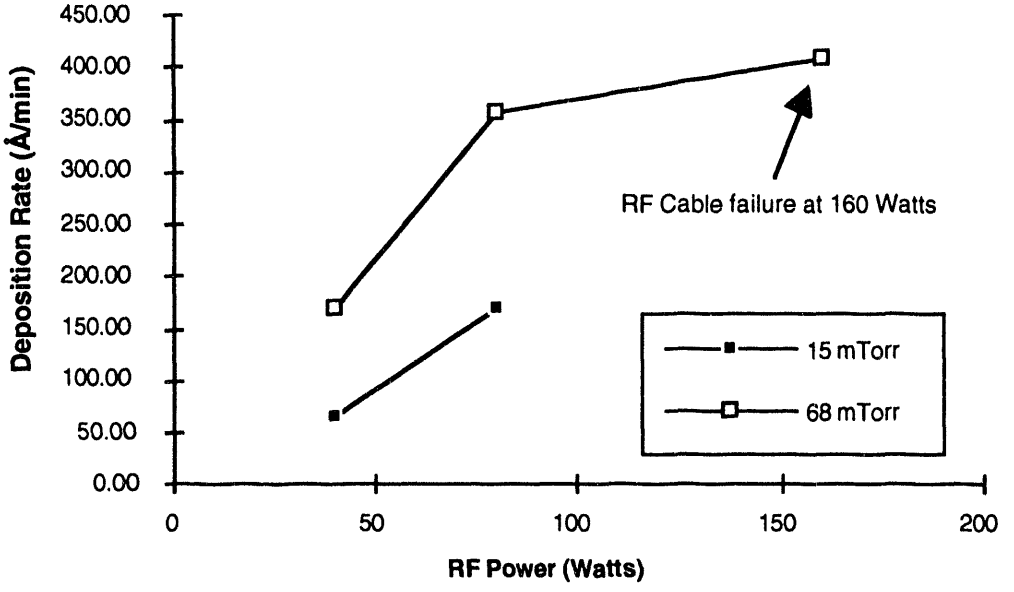

Figure 2.1. The effect of RF power and methane pressure on deposition rate.

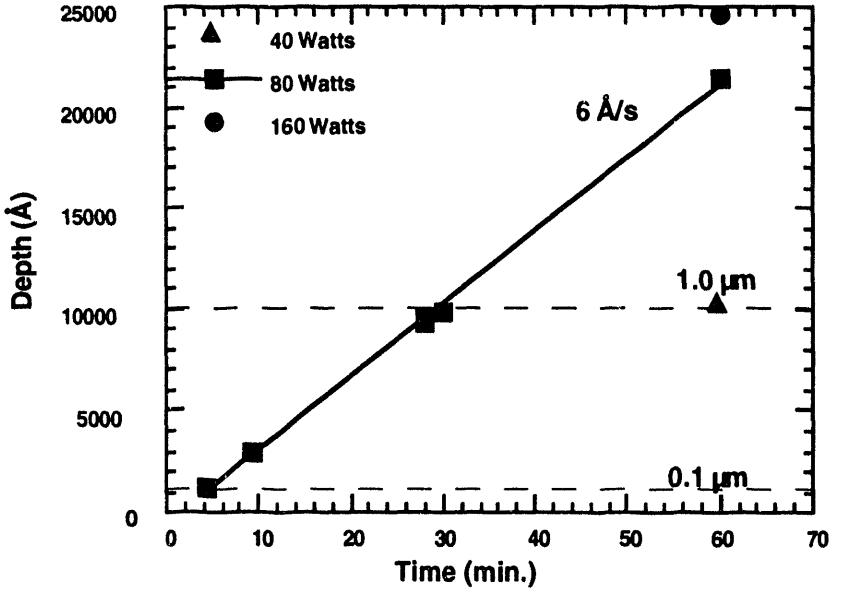

Figure 2.2. DLC depth versus deposition time.

3.0 DLC-Substrate Compatibility - Duane Outka

The modest deposition temperature (≤100° C) of the PECVD process permits DLC to be deposited onto a variety of substrates. The major limitation regarding substrate compatibility with DLC is whether the DLC coating will adhere well. **Table 3.1** presents a list of substrates for which DLC has been successfully deposited using the PECVD reactor, (the structural formulas for the organic substrates are given in **Fig. 3.1.**) In all these cases, DLC coatings have been deposited and remained adherent for a period of several months. In some cases, DLC does not adhere well directly to the substrate (e.g. stainless steel), but adherent coatings have been achieved by using an interlayer material to enhance adhesion as discussed below in section 8.

Table 3.1 List of DLC Compatible Substrates

Alumina	Molybdenum
Aluminum	Polycarbonate (Lexan)
5053 aluminum alloy	Polyethylene
6061-T6 aluminum alloy	Silicon
Anodized aluminum	15-5 PH stainless steel*
el-dep-anodic acrylate clear resin on anodized 6061 aluminum**	303 Se stainless steel*
	304 stainless steel*
Graphite	440 stainless steel*
Iron*	Tantalum
Kevlar	Tungsten

* Using silicon interlayer to improve adhesion.

** The el-dep-anodic acrylate clear resin is a commercially-available, electro-deposited, form of poly(styrene acrylate).

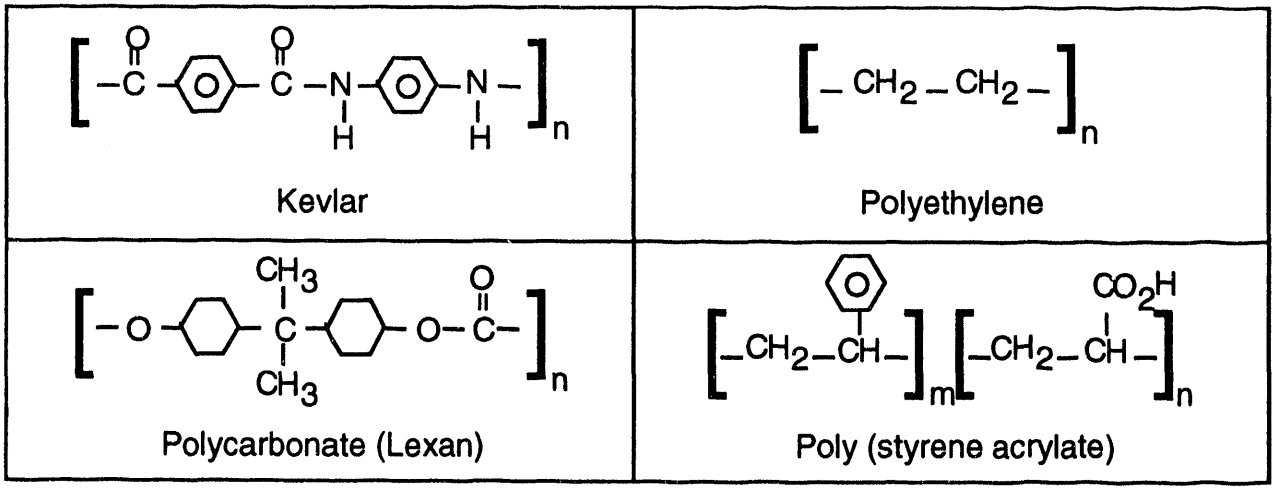

Figure 3.1. Structural formulas for selected compounds listed in Table 3.1.

Table 3.2 lists materials on which DLC has not yet been successfully deposited. In these cases, the DLC either did not form or delaminated shortly after deposition. In some of these cases it may be possible to achieve adherent coatings by further optimization of the deposition process or use of an interlayer.

Table 3.2 List of DLC Incompatible Substrates

Copper
Gold
Nickel

4.0 Chemical Resistance of DLC Coatings - Dale Boehme

The chemical inertness of diamond makes its use attractive as a protective coating against chemical attack. Although diamond will oxidize at high temperatures, or dissolve in carbide forming metals, it is otherwise inert. DLC is expected to be chemically unreactive like diamond [8]. Chemical resistance characterization of the DLC films produced in this study involved the measurement of resistance to several concentrated acids including hydrochloric, sulfuric, and nitric.

Aluminum alloy substrates were chosen as test coupons for DLC deposition, because of the common use of aluminum and aluminum alloys in weapon applications and general manufacturing. Aluminum and its alloys react with most acids and were used as the indicator for acid penetration through the DLC coating. Two inch diameter disks of 6061-T6 and 5053 aluminum, 1/4" thick, were metallographically polished to a 0.5 micron finish using a silica slurry and cleaned with isopropyl alcohol. After deposition of DLC layers, the specimens were tested by placing drops of acid on the surface and recording any observation of chemical attack to the Al by permeation through the coating as a function of time (**Fig. 4.1**).

The first test samples produced consisted of single, 1-2 micron thick layer of DLC deposited on the Al substrates. Immediate reaction occurred with the Al substrate (< 10 seconds) for the three acids tested (**Figs. 4.2 and 4.3**). Analysis using optical and SEM microscopy revealed the presence of tiny pin-holes (< 1 micron) which were present in the deposited coating. Further examination using SEM suggested that the holes were produced by stress cracking around inclusions present in the aluminum and exposed at the substrate surface (**Fig. 4.4**). Al-6061-T6 contains insoluble $(Fe,Cr)_3SiAl_{12}$ inclusions and excess Mg_2Si particles that are harder than the matrix and, therefore, would stand in relief on the polished surface (**Fig. 4.5**). Al-5053 can contain inclusions of Mg_2Al_3 and Mg_2Si, but they are not as abundant.

Although DLC produces a relatively conformal coating, small features on the Al substrates sometimes caused defects in the deposited layer. Hydrochloric acid was used to detect these defects. The DLC coatings itself was resistant to attack by the hydrochloric acid, but the substrate reacted with hydrochloric acid. This attack occurred at defects in the coating where the acid could reach and attack the underlying substrate.

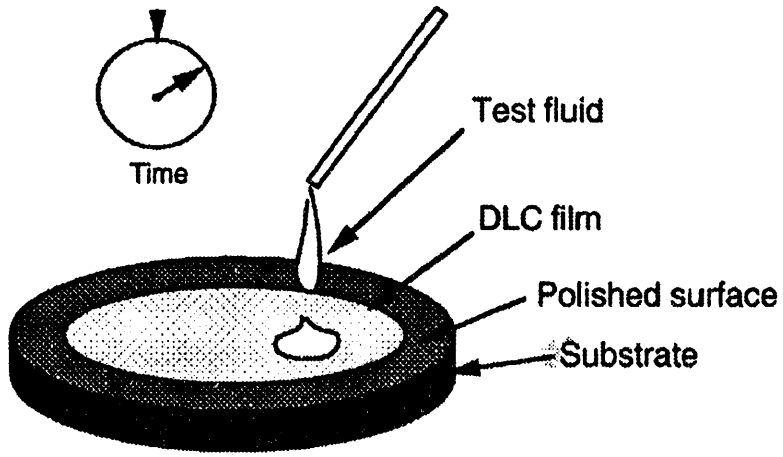

Figure 4.1. Diagram representing chemical test procedure.

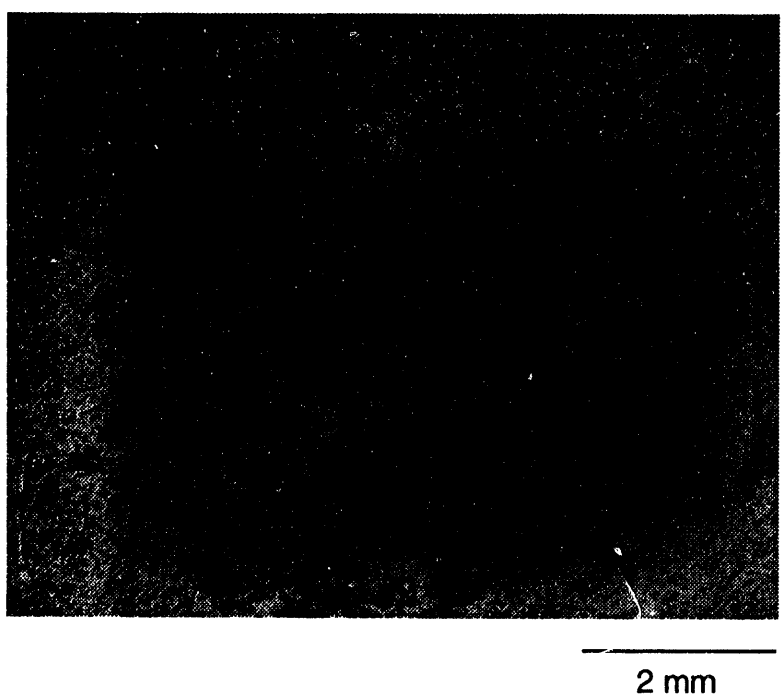

Figure 4.2. Micrograph showing area of DLC coating exposed to HCl. Dark patches are where the DLC corroded away resulting from HCl reaction with the Al-substrate after permeating through pin-holes.

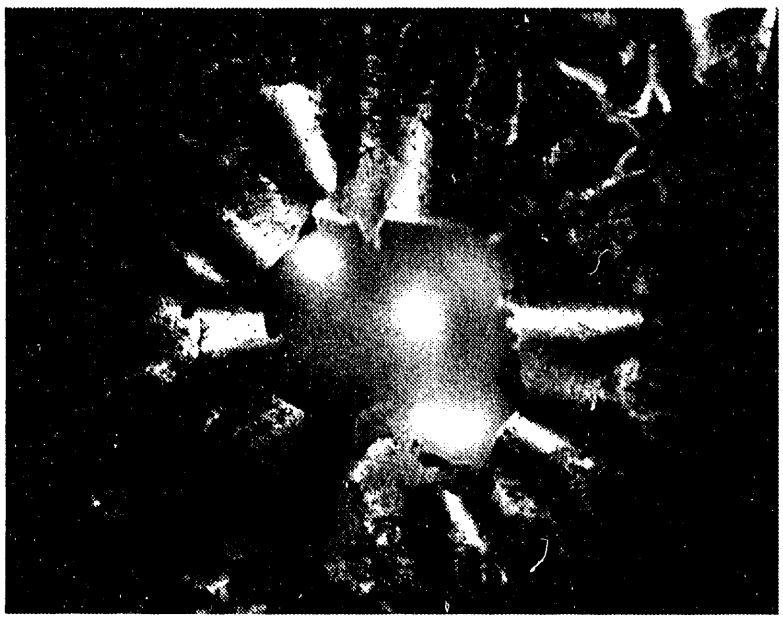

Figure 4.3. Individual defect produced by reaction of HCl with Al substrate showing delamination of the coating as HCl/substrate reaction progresses.

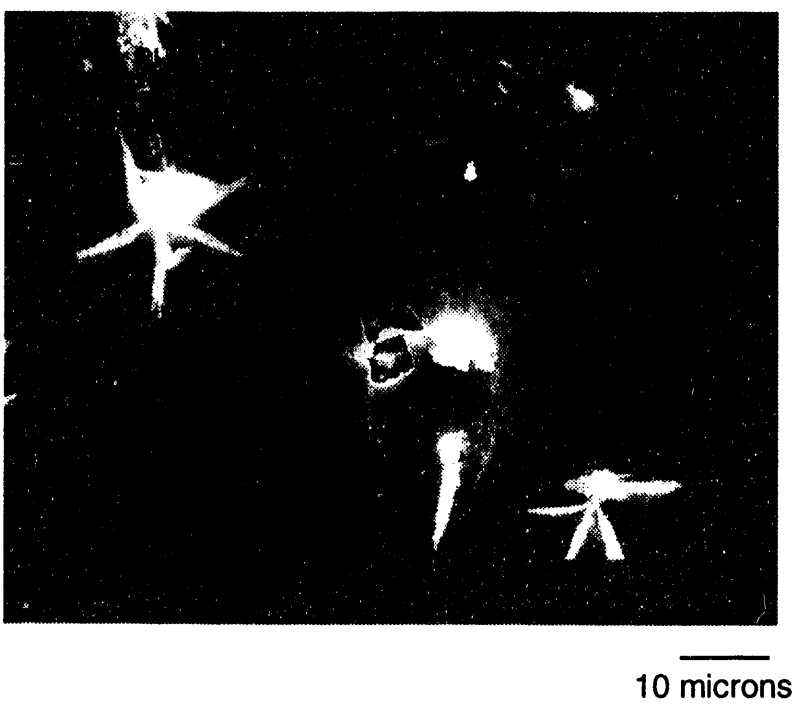

Figure 4.4. SEM micrograph showing stress cracking and pin-hole formation.

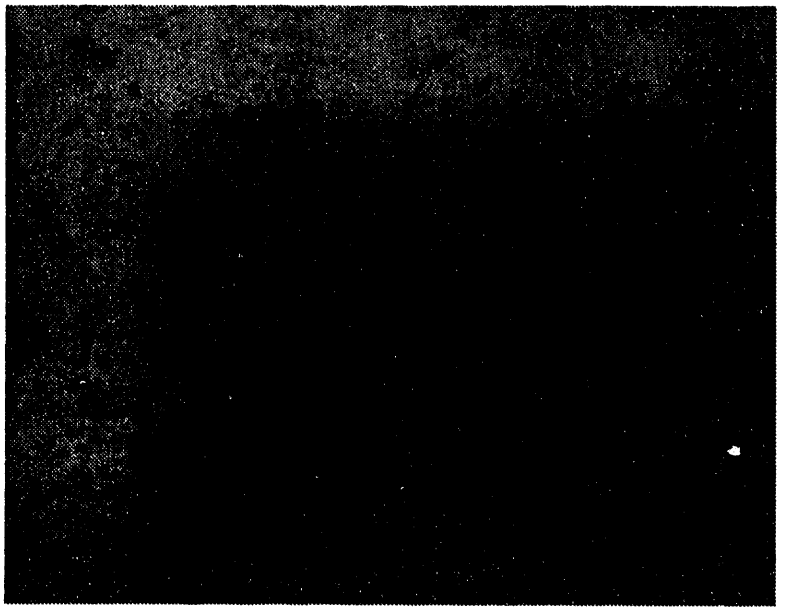

Figure 4.5. Optical micrograph showing inclusions exposed on the surface of an Al-6061-T6 polished disk.

Various efforts were made to eliminate defects in the DLC coating including use of thicker coatings (up to 2 microns), multiple layered coatings, and a silicon inter-layers. None of the coating were entirely free from defects, however. Thicker coatings were relatively more resistant to chemical attack than thinner coatings since they increased the time for acid permeation through the layer. For example, with the thinner coatings, reaction between the Al substrate and the acid was immediate. Thicker coatings delayed reaction up to 5 minutes although there was some evidence of permeation almost immediately. Using multiple layered coatings (consisting of both thin and thick layers, 0.5 micron and 1.5 micron, respectively) the resistance to reaction increased up to 20 minutes. Coatings with a silicon layer between the DLC and Al substrate provided the best resistance to permeation, delaying reaction with the substrate for up to 1 hour (**Fig. 4.6**). However, while the permeation time slowed down even more, the effect of permeation was not entirely eliminated using the Si inter-layer, because of the continued presence of coating defects.

From these investigations several factors are important. Cleanliness of the substrate prior to deposition is vital. This includes cleanliness of the sample chamber itself during the deposition process to prevent the encapsulation of dust particles or other debris into the DLC film which could result in defects. Surface roughness and/or defects (i.e., inclusions at the surface) may be an issue related to stress and pin-hole formation. This can possibly be eliminated by using an interlayer between the DLC and substrate, but more investigations are required to corroborate this.

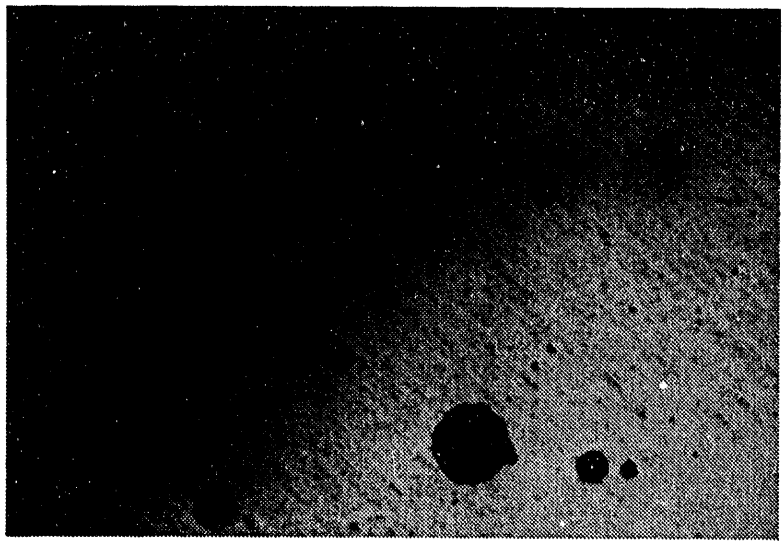

Figure 4.6. Micrograph of Al-6061-T6 polished disk with DLC coating with a silicon inter-layer—after exposure to concentrated HCl. Dark spots show where acid has permeated through pin-holes in the coating and reacted with the underlying substrate.

5.0 Electron Microscope Analysis of DLC Coatings - Nancy Yang, Thomas J. Headley, and Miles Clift

Optical microscopy, electron microscopy, and electron-based analysis including SEM (scanning electron microscopy), HRTEM (high resolution transmission electron microscopy), FESEM (field emission scanning electron microscopy), EDS (energy dispersive X-ray spectroscopy), and AES (Auger electron spectroscopy) have been useful in examining the structure, bonding, and adhesion of DLC films to various substrates. This section presents several studies of DLC coatings using these techniques and illustrates the types of problems which must be overcome to obtain successful coatings with DLC and the type of information available with these techniques.

5.1 HRTEM Study of DLC

DLC has a hardness and coefficient of friction which approaches that of diamond. The structure of DLC, however, is different from that of crystalline diamond. This study examines the structure of DLC with HRTEM and demonstrates the amorphous nature of DLC films.

The sample was a flake of DLC which peeled from a ceramic insulator following deposition of DLC. The DLC flake was examined with a Philips CM30 TEM with twin lenses and operated at 300 kV. The instrument has a point-to-point resolution at Sherzer defocus of 2.3 Å. HRTEM images of the amorphous films were taken at a defocus values exhibiting maximum contrast of the granular appearance of the amorphous DLC which corresponds approximately to Sherzer defocus. HRTEM images of crystalline material were taken at a defocus value exhibiting

approximately maximum contrast of the lattice fringes in the image. This defocus value depends on fringe spacing and is not generally at Sherzer defocus.

Fig. 5.1.1 shows a typical HRTEM image of DLC taken at a magnification of 2,600,000 times. There is no evidence of crystallinity which demonstrates the amorphous nature of DLC.

Small regions of the sample did show evidence of crystallinity due to impurities as shown in **Fig. 5.1.2** (region A). EDS showed that the ordered regions were not composed of carbon, but contained aluminum, calcium, fluorine, and oxygen. It was therefore concluded that these ordered region were simply an impurity on one side of the sample stripped from the substrate before the DLC flaked off.

5.2 Analysis of Adhesion Failure of DLC to Iron using SEM

DLC coatings on iron and stainless steel are of interest as a lubricating and protective coating. Based upon a consideration of the chemical aspects of adhesion in section 8, however, DLC is expected to have poor bonding to iron. Our experiments of DLC deposition on iron substrates confirmed this poor adhesion. Microscopic analysis of the DLC coatings on iron was undertaken in order to understand in more detail the adhesive failure of these coatings.

A 2 inch diameter iron wafer was coated with an approximately 0.5-μm-thick coating of DLC. After a period of hours, coating failure became apparent near the edges of the coating. This failure region increased in extent with time. **Fig. 5.2.1** shows an optical micrograph of a pie-shaped wedge cut from the wafer. The light areas near the edge of the coating are areas of failure while in the dark region, the coating is still adherent. The region around E was masked during deposition and was uncoated. Coating failure occurred both at the edge between the coated and uncoated regions (edge C) and along the edges where the wafer was cut (edges A and B). A light oval spot is also seen in **Fig. 5.2.1** where coating failure occurred (point D). This is an artifact due to laser beam damage, however, caused by another experiment unrelated to the current discussion.

Differences in the width of the failure zones along the edges of the sample provide insight into the mechanism of adhesive failure. In particular, the size of the failure zones has the following order C > B > A. The extent of failure along the edges correlates with the presence of fine, parallel grooves present on the face of the sample due to the mechanical rolling or machining of the iron substrate sheet. The direction of these grooves is roughly parallel to edge A in **Fig. 5.2.1**. Failure of the coating appears to proceed rapidly along the direction of the grooves (e.g. at point C), but is slow in the direction perpendicular to the grooves (e.g. edge A). This is shown more clearly in the optical micrographs shown in **Fig. 5.2.2**. Areas of failure appear white in this figure and appear to align with the machining grooves in the substrate.

Optical microscopy lacks the resolution and depth of field to examine the morphology of the DLC coating in great detail. The DLC coatings were also examined with conventional SEM, but at 15 KV accelerating voltage, the electron beam penetrates too deeply (>> 1 μm) to be coating sensitive. The result is that SEM provides little detail regarding the morphology of the DLC

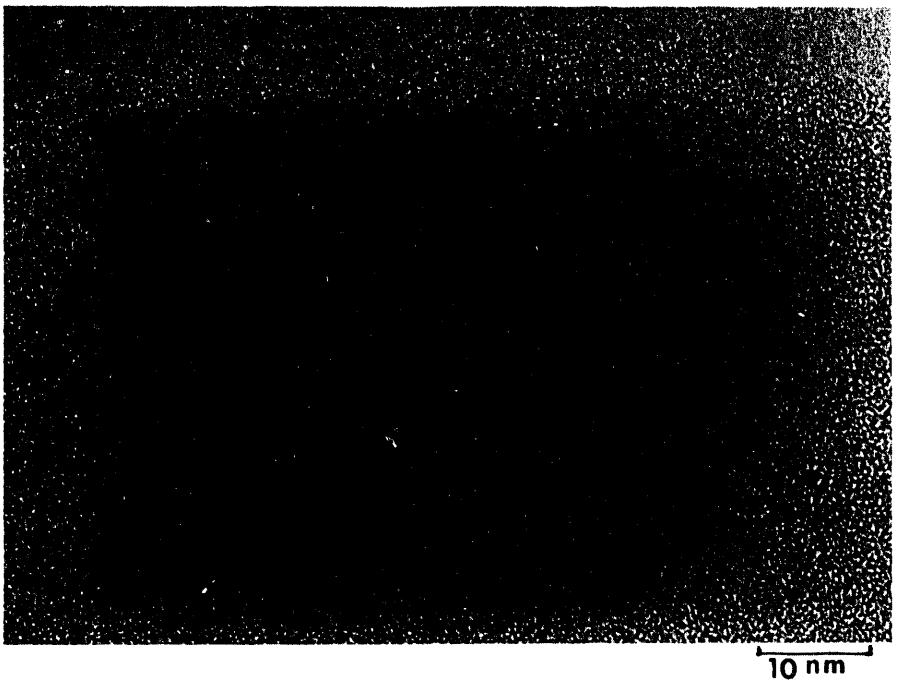

Figure 5.1.1. HRTEM showing amorphous nature of DLC.

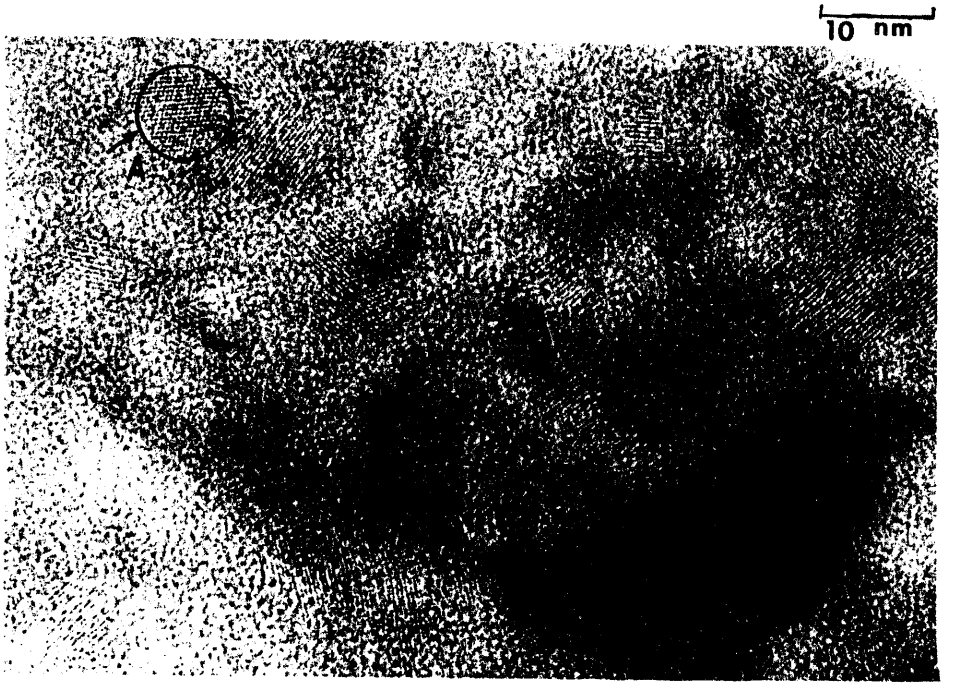

Figure 5.1.2. DLC with some impurities that contain crystallinity as shown by arrow A.

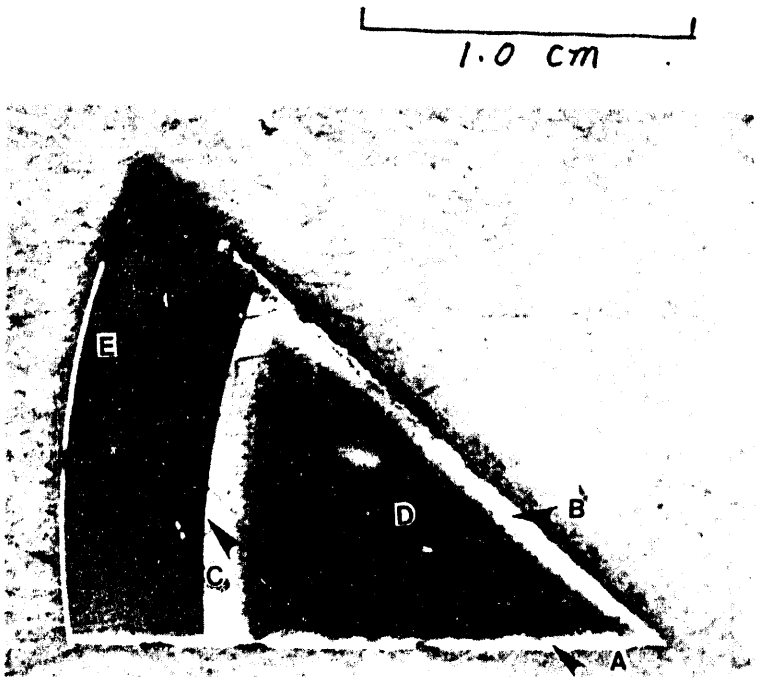

Figure 5.2.1. This optical image shows regions of coating failure (light regions A, B, C) in comparison to the adherent region (dark center). Region E is the uncoated portion of the steel wafer.

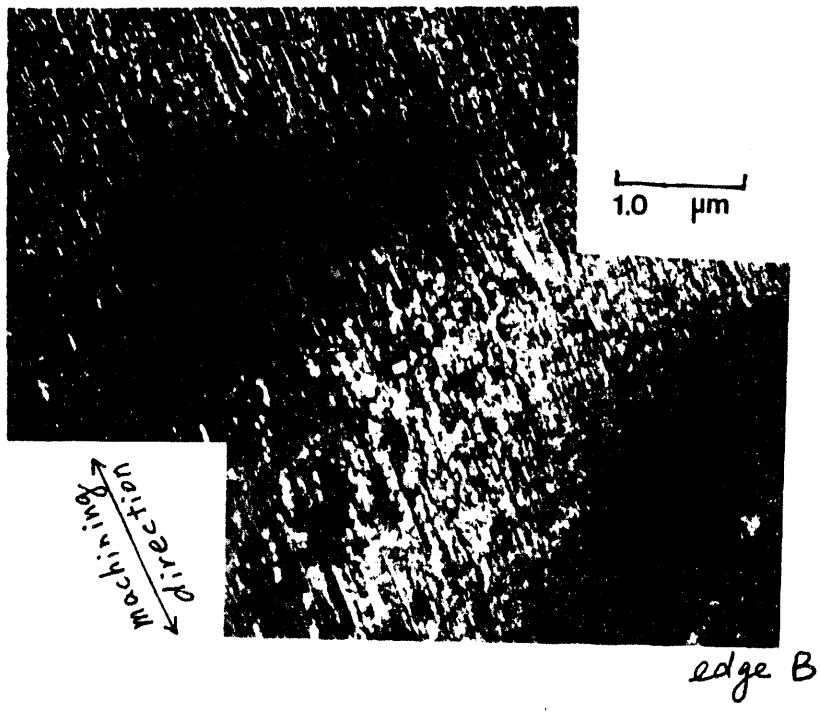

Figure 5.2.2. Optical image shows that the failure (light spots in this figure) proceed along the direction of the grooves.

coating. The morphology of the DLC coatings could be successfully examined with FESEM which uses a primary electron beam of only 2.5 KV. This technique examines the SEI (secondary electron image) to achieve surface sensitivity.

FESEM demonstrates that coating failure begins as discontinuous patches near the interior of the sample which join and eventually cause flaking of the coating near the coating edges. **Fig. 5.2.3b** shows incipient coating failure near the interior of the sample. Failure appears as discreet bubbles of DLC whose interior has become detached from the surface. In these bubbles the coating is raised above the surface of the sample which indicates the presence of compressive stresses in the coating. This is consistent with stress measurements discussed in section 7.3. In the early stages of coating failure, the bubbles are small and discontinuous (point A in **Fig. 5.2.3b**), but neighboring patches tend to be aligned along the sample grooves. In **Fig. 5.2.3a**, the bubbles have joined together to form large patches of delaminated coating. Eventually, these large areas of detached DLC can break and flake off the substrate entirely. **Fig. 5.2.3a** also shows that cracks in the coating tend to start along the groove lines of the substrate (point B).

There are several explanations for the correlation between coating failure and the grooves in the sample. One possibility is the grooves provide a pathway for air and moisture to reach between the iron and the coating and thus leads to coating failure. Another possibility is that the structure of the grooves, lead to sites of stress concentration, which leads to coating failure.

5.3 Analysis of Adhesion of DLC to 303 Se Stainless Steel using SEM

DLC deposition on various stainless steels is of interest as a tribological coating in mechanical applications because of DLC's hardness and low coefficient of friction. DLC, by itself, adheres poorly to stainless steels, however, so use of a silicon interlayer has been developed at Sandia to improve the adhesion of DLC to stainless steels (see section 8). The use of a silicon interlayer was initially demonstrated using sputtered silicon interlayers. Sputtered silicon interlayers are limited to line-of-sight deposition, however, which would negate one of the prime advantages of plasma deposited DLC which is its conformal coating capability (i.e. not line-of-sight). One alternative to using sputtered silicon interlayers, which was investigated, was to use CVD (chemical vapor deposition) deposited silicon interlayers. To accomplish this, an outside company was contracted to deposit silicon interlayers using a CVD process. The samples were then coated with DLC using our conventional PECVD process. Unfortunately, the resultant film was poorly adherent so the film was examined by various microscopic and electron-based analytical techniques to understand this failure.

The substrate material was 303 Se stainless steel for which a hard protective coating was desired. The sample was a 1 inch diameter disk and was polished smooth to within 20 nm RMS roughness. This was coated with 0.1 μm thick amorphous silicon by an outside vendor. The sample was then coated with approximately 0.5 μm of DLC using Sandia's conventional PECVD process. The resultant films were poorly adherent with obvious flaking of the coating. Optical microscopy (**Fig. 5.3.1**) shows the flakes on the surface of the sample and areas where the coating has been delaminated entirely. The flakes on the surface are curled which is indicative of high stresses in the films and likely contributed to film failure. Adherent DLC coatings have high stress as well, however, so there must be other contributing causes to the DLC film failure.

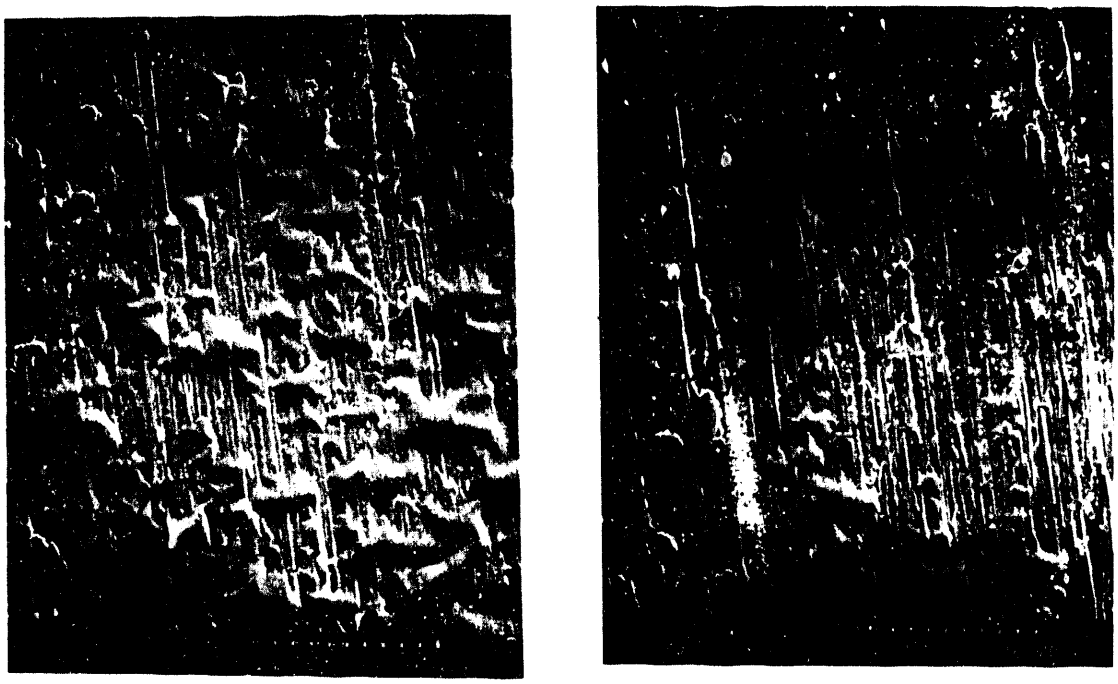

Figure 5.2.3. Typical image shows of discolored area. Bubbles correspond to the film lifted areas. (a) - Extensive film failure near the coating edge, (b) - Incipient film failure toward the coating interior.

Figure 5.3.1. (a): Optical micrograph showing DLC flakes peeling off the substrate (130x). The DLC film is still adherent in the dark region. (b): SEM micrograph showing loose DLC flakes (100x).

EDS examination of the flakes indicates that failure of the coating occurred at the stainless steel-silicon interface. With EDS, a single flake can be examined and the spectrum shows that one side of a flake was silicon rich whereas the other side was carbon rich (**Fig. 5.3.2**). The presence of silicon on the flake indicates that the silicon-DLC bonding was intact, but that the stainless steel-silicon bonding had failed. Furthermore, it was the concave side of each flake that was silicon rich which is consistent with the compressive stresses typically found in DLC coatings.

Auger depth profiling further indicated that failure occurred at the stainless steel-silicon interface. Depth profiling was performed in regions on the same sample where film failure had occurred and also regions where the film was still adherent. Auger spectroscopy found oxygen in a range of 2 to 10% at the stainless steel-silicon interface (**Fig. 5.3.3**). Furthermore, the Auger peak position of the Si (KLL) transition indicated that the oxygen was associated with the iron and not the silicon. There was no oxygen within the silicon interlayer, however, which rules out the possibility that the silicon layer was oxidized by exposure to air between deposition of the silicon and DLC layers. Instead, failure is localized at the stainless steel-silicon interface. Auger scans of the flakes also found evidence of iron on one side of the flakes, further supporting the idea that failure occurred at the stainless steel-silicon interface.

The presence of Se inclusions at the surface of the stainless steel was also apparent using SEM and Auger electron spectroscopy. The Se is a deliberate component of the 303 Se stainless steel which improves its machinability. Se enriched particles with dimensions of about 1 μm were observed on the surface of the steel substrate. The effect of Se on adhesion is not clear, however. In some cases it appeared that failure of the DLC coating occurred near the Se inclusions, but in other cases, the DLC covered a Se inclusion with no indication of film failure. It appears that silicon and DLC does not adhere as well to the Se as to the iron component of the substrate and thus weakens the adherence of the film. It is not likely the primary cause of the DLC film failure, however.

From these results the primary cause of the film failure was determined to be oxygen contamination at the stainless steel-silicon interface. This combined with the high compressive stresses in the DLC film led to flaking off of the DLC and silicon coating. It is speculated that the stainless steel substrates were not adequately cleaned by the the outside vendor. before deposition of the silicon interlayer. Oxidation of the entire silicon interlayer has been ruled out as a cause of the film failure, because oxygen was not incorporated into the silicon interlayer itself according to Auger depth profiling measurements. It is also known that adherent DLC films can be deposited onto 303 Se at Sandia using in-situ argon ion cleaning and sputtered silicon interlayers so there does not appear to be a chemical problem in the bonding of DLC to silicon to 303 Se stainless steel. These results highlight the difficulty of achieving good quality films unless detailed cleaning and deposition conditions are specified and verifiable.

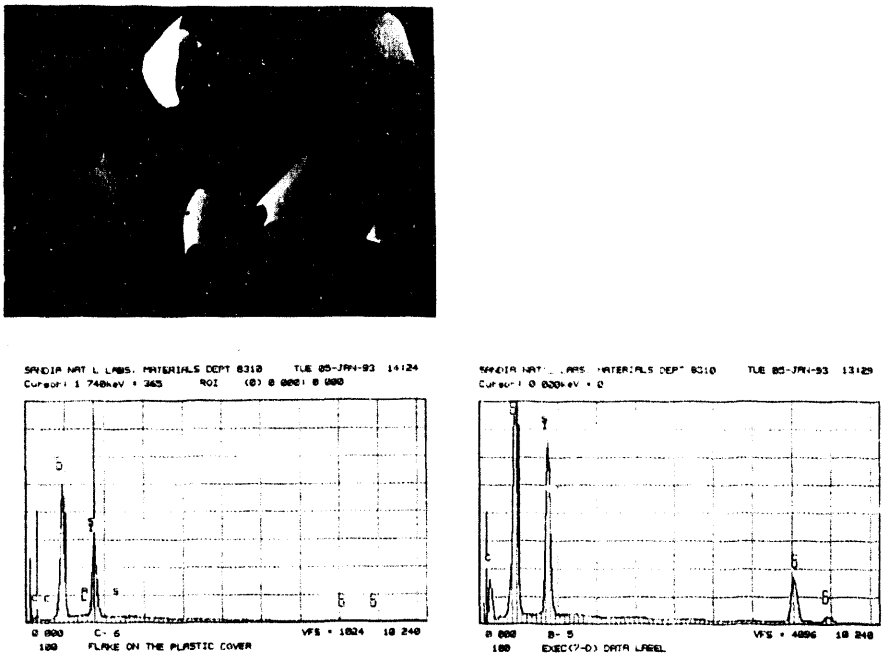

Figure 5.3.2. (a): Typical bent flakes. (b): No carbon was detected on the concave side indicating it is from the Si-stainless steel interface. (c): Carbon was detected on the convex side indicating it is the DLC surface.

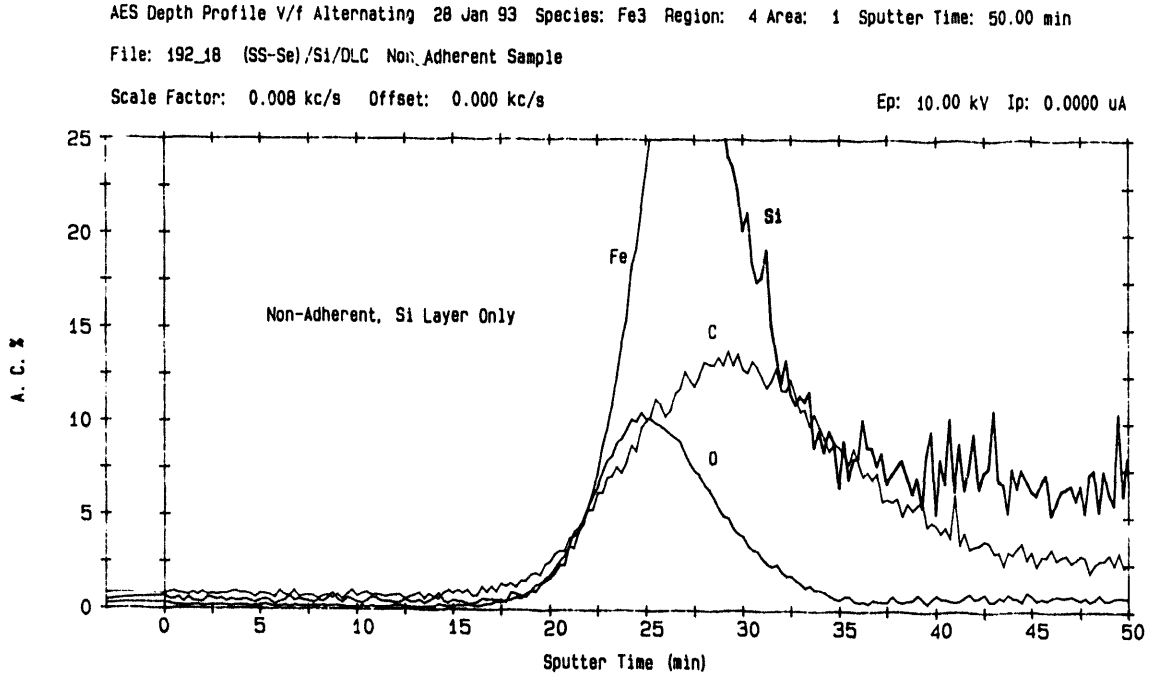

Figure 5.3.3. AES depth profile of failed DLC coating on 303 Se stainless steel showing oxygen impurity at Fe-C interface.

6.0 FTIR Studies of DLC Coatings - Dave Ottesen and Howard Johnsen

FTIR (Fourier Transform Infrared) reflectance spectroscopy has been used to examine the bonding and the thermal stability of DLC coatings on a Si(100) substrate. The spectra were measured with a Biorad FTS-60A instrument with a grazing angle of incidence (60°) and a p-polarized beam. Spectral resolution was approximately 4 cm^{-1}. All reported reflectance spectra have been divided by a reference reflectance spectrum of a bare silicon substrate in order to remove instrument response function and spectral structure due to the substrate material.

Three samples were examined with starting DLC thicknesses ranging from 0.395 to 2.140 μm. Before deposition the samples were cleaned in-situ using an argon plasma etch. The DLC was deposited using RF plasma enhanced chemical vapor deposition from methane. The table below lists the three samples examined and the starting thicknesses of the DLC coatings as measured by profilometry.

Sample Number	DLC Coating Thickness
KP06/28/93.W1	0.4 μm
KP06/29/93.W1	1.0
KP06/29/93.W2	2.1

Divided FTIR reflectance spectra of DLC on Si(100) covering the spectral region from 2000 - 3500 cm^{-1} are shown in **Figs. 6.1** through **6.3.** The spectra are shown as a function of annealing to various temperatures as discussed below. Major features of the spectra are: (1) a large amplitude sinusoidal fringe pattern which varies in wave number spacing with film thickness, and is due to multiple reflectance interference within the thin DLC films; (2) absorption features near 2900 cm^{-1} due to C-H stretching modes characteristic of sp^3 hybridization; (3) and a small residual feature near 2350 cm^{-1} due to atmospheric carbon dioxide whose absorption was imperfectly compensated during dividing of the sample and reference reflectance spectra. In addition, no pronounced change in the reflectance of the samples was observed near 1100 cm^{-1} indicating the absence of oxidation of the substrate near-surface region.

Of particular interest in the FTIR spectra is insight into the nature of the hybridization of carbon in the DLC films (i.e. the sp^3/sp^2 ratio). The C-H stretching features are below 3000 cm^{-1} indicating that some of the carbon is sp^3 hybridized like diamond. Unfortunately, infrared spectroscopy is rather insensitive to C-H stretches for carbon with sp^2 hybridization because of the small dipole moment change. Thus, no conclusions can be made regarding the sp^3/sp^2 ratio in DLC. Also, the C-C stretching mode is not observed because of the absence of a dipole moment change.

The thermal stability of DLC in air was examined by heating the samples to various temperatures and monitoring the FTIR and weight change in the samples. The samples were heated to successively higher temperatures for two hours in an atmosphere of ambient air. After each heating cycle the FTIR spectrum was measured and weight changes were recorded after the samples cooled. Weight changes are given in the following table relative to the starting weight.

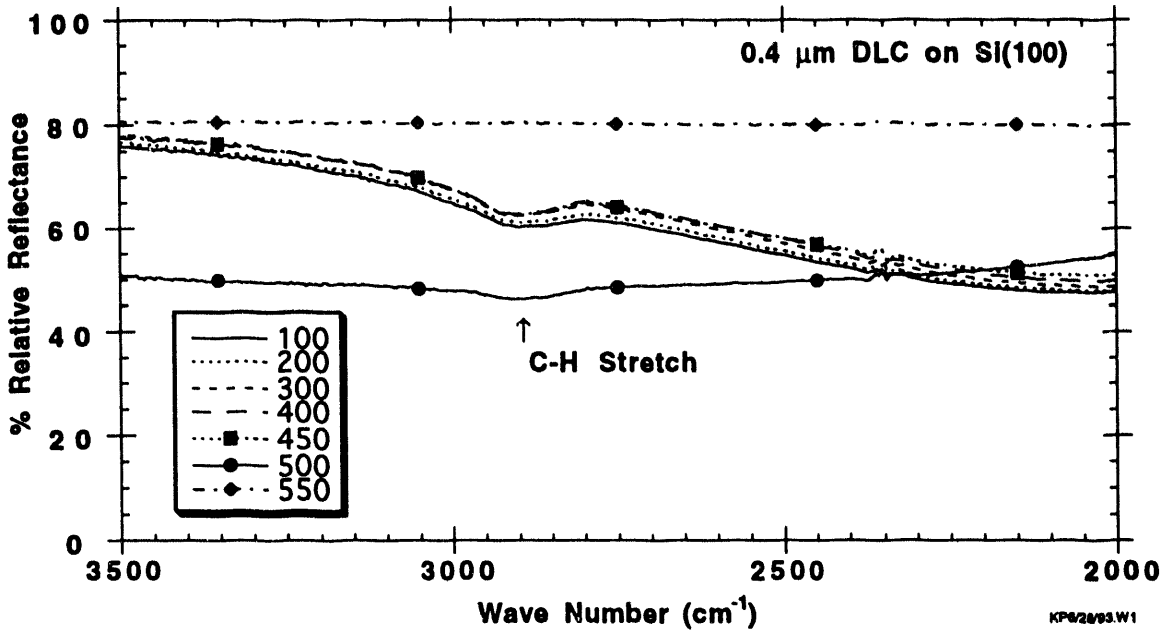

Figure 6.1. FTIR spectra of a 0.4 μm thick DLC film on Si(100) heated to various temperatures up to 550° C.

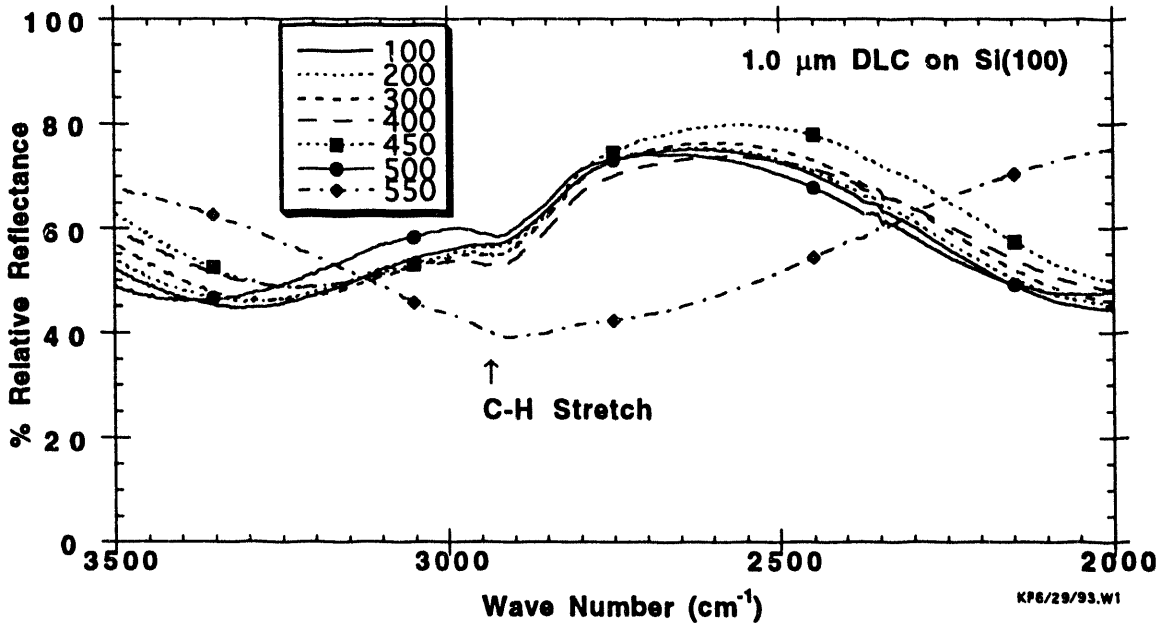

Figure 6.2. FTIR spectra of a 1.0 μm thick DLC film on Si(100) heated to various temperatures up to 550° C.

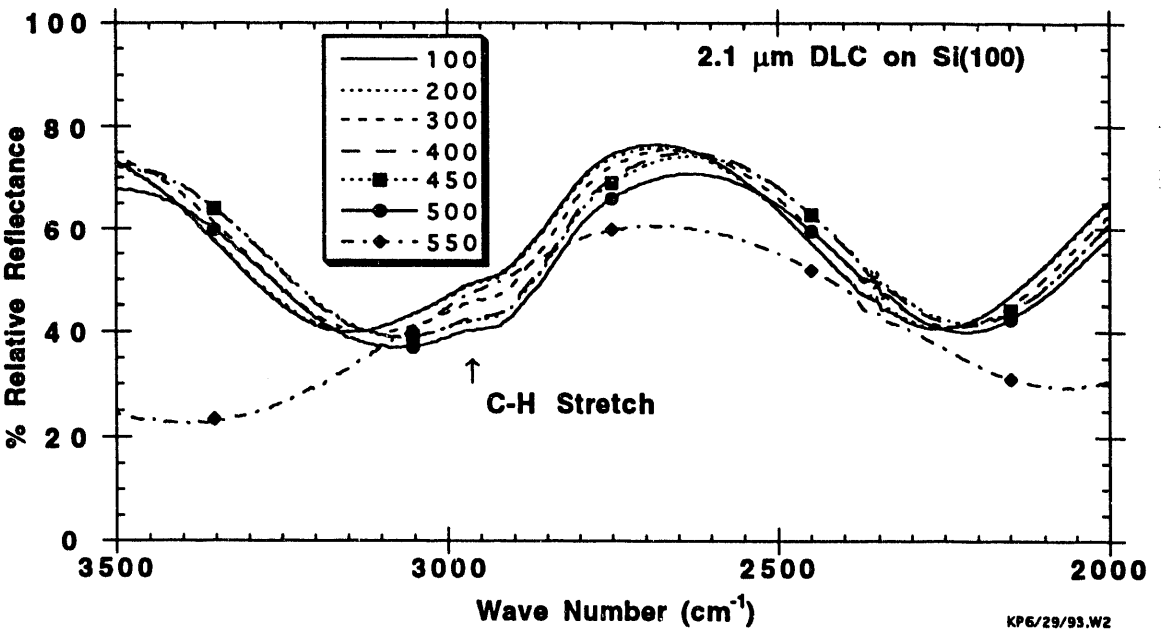

Figure 6.3. FTIR spectra of a 2.1 µm thick DLC film on Si(100) heated to various temperatures up to 550° C.

Temperature	0.4 µm sample	1.0 µm sample	2.1 µm sample
100° C	0.0 mg	0.0 mg	0.0 mg
200° C	0.0 mg	0.0 mg	0.0 mg
300° C	0.0 mg	0.0 mg	0.0 mg
400° C	0.0 mg	0.0 mg	0.0 mg
450° C	-0.2 mg	0.0 mg	0.0 mg
500° C	-1.4 mg	-0.8 mg	-0.4 mg
550° C	-2.9 mg	-3.5 mg	-5.6 mg

The results indicate that DLC is stable in air up to approximately 450° C. Below this temperature little or no weight change was observed. There was a small consistent increase, however, in the interference fringe frequency for each DLC sample with increasing temperature. This could be caused either by increasing film thickness or increasing index of refraction of the film.

Above approximately 500° C oxidation of the DLC was observed. Large changes in the interference fringe are observed at 500° C for the thinnest film, and at 550° C for the two thicker films. This spectral change coincides with observed major weight losses. In addition, there are changes in the C-H stretching feature. For the 0.395 µm DLC film, the C-H stretching feature and the film interference fringe are greatly diminished after the 500° C heating and are completely absent after the 550° C heating. For the two thicker DLC films, the C-H stretching feature and interference fringe show small changes after heating at 500° C, and are notably diminished (but not completely absent) following the 550° C heating.

Total weight changes after heating at 550° C are not proportional to initial film thicknesses. This may be due to patches of residual DLC film on the silicon substrate even after final heating. This is suggested by visual appearance as well as the spectral data in the figs. 6.1 through 6.3.

Further analysis of the spectral data will use curve fitting to remove the interference fringes and enhance the observed changes in C-H stretching absorptions. These results will be reported in a later document.

7.0 Stress in DLC Films - Duane Outka and Kristen Phillips

7.1 Sources of Stress in DLC Films

Stress is an important property of DLC coatings because stress leads to poor adhesion. Furthermore, stress is a mechanical property which can be readily measured. As in bulk materials, the fracture at an interface is determined in large part by mechanical properties. In general, however, the details of fracture at an interface and how it relates to the microscopic structure and morphology of a film is unknown. The only mechanical property of DLC films which has been investigated in detail and which affects adhesion is stress. Although there is not a simple relationship between stress and adhesion, stress is undesirable because it can cause buckling or cracking of the thin film and thus adhesive failure. Stress in thin films is divided into two types: thermal and intrinsic.

The **thermal** stress at an interface can be readily predicted (see for example Hoffman [9] and Chopra [10]). Thermal stress is a particularly difficult problem for DLC and diamond films because of the small coefficient of thermal expansion of diamond (**Table 7.1**); it is smaller than any other material in the table. (The thermal properties of DLC are poorly characterized and, therefore, those of diamond will be used as an approximation for DLC.) Thus if diamond films are deposited on a substrate at elevated temperature, then cooled to room temperature, the substrate will contract by a greater amount than the diamond overlayer. Since the diamond film is bonded to the substrate, the interface area will change to match that of the substrate resulting in the development of compressive stress in the diamond film.

The stress due to thermal expansion mismatch between a substrate and overlayer can be calculated using

$$\sigma = \frac{E\,(\alpha_f - \alpha_s)\,\Delta T}{(1 - \nu)} \qquad (2)$$

where σ is the stress; E is the elastic modulus of the film; α_f and α_s are the average coefficients of expansion for the film and the substrate, respectively; ΔT is the temperature change between deposition and measurement; and ν is Poisson's ratio for the overlayer. Consider, for example, a DLC film deposited at 100 °C on a silicon substrate with a measurement at 20 °C. Assuming that the thermal coefficient of expansion of the DLC film is the same as diamond and that Poisson's ratio is 0.2 [17], the stress in the thin film is calculated to be 1.4×10^8 Pa and is compressive. This is somewhat smaller than the range of measured stress values for DLC films on silicon which vary from $5. \times 10^8$ to $4. \times 10^9$ Pa (see **Table 7.2**). The measured stresses may be

larger than the calculated stress for several reasons. First, the temperature rise of the substrate may be higher than commonly believed because of difficulties of temperature measurements during deposition. Second, the mechanical properties of a DLC film may differ from that of bulk diamond which were used in the calculations above.

Table 7.1 Mechanical and Thermal Properties of Materials

Material	Linear Coeff. of Thermal Expansion (at 20 °C) $\times 10^{-6}$ °C^{-1}	Modulus of Elasticity $\times 10^{11}$ Pa	Density (g cm^{-3}) (at 20 °C)
Aluminum	23. [11]	0.706 [12]	2.702 [13]
Al_2O_3	approx. 5.3 [11]	4.0 [14]	3.965 [13]
Chromium	5.0 [11]	2.79 [12]	7.20 [13]
Copper	16.7 [11]	1.298 [12]	8.92 [13]
Diamond	1. [11]	9.1 [14]	3.51 [13]
Germanium	5.7 [11]		5.35 [13]
Glass	4. to 9. [11]	0.48-0.83 [15]	
Graphite	7.8 [11]		2.25 [13]
Iron	11.8 [11]	1.523-2.114 [12]	7.86 [13]
Molybdenum	5.0 [11]	3.248 [12]	10.2 [13]
Nickel	12.8 [11]	1.995-2.192 [12]	8.9 [13]
Platinum	8.9 [11]	1.67 [11]	21.45 [13]
Silicon	2.5 [11]	6.6 [16]	2.33 [13]
SiC	3.7 [11]	4.8 [14]	3.217 [13]
SiO_2	approx. 11.2 [11]		2.64 [13]
NaCl	42.3 [11]		2.165 [13]
Stainless Steel	15.9 [11]	2.153 [12]	
Titanium	8.6 [11]	4.7 [14]	4.5 [13]
TiC	6.2 [11]		4.93 [13]
Tungsten	4.5 [11]	4.11 [12]	19.35 [13]
Uranium	14.1 [11]		19.05 [13]

Stresses in thin films can also differ from that predicted by thermal expansion because of **intrinsic** stress. Intrinsic stress is related to the structure and morphology of the deposit. Unfortunately, this type of stress is poorly understood. In principle, intrinsic stress can be reduced by optimizing deposition conditions.

7.2 Previous Studies of DLC Film Stress

Stress in DLC films is important because it can lead to buckling or cracking of the coating. Angus [6] and Tsai and Bogy [18] briefly review the issue of stress in DLC and diamond films. In contrast to adhesion, stress in films can be quantitatively measured. Usually this is performed by the beam deflection method which is discussed by Campbell [12]. **Table 7.2** list the studies where quantitative measurements of the stress for DLC or diamond films have been reported. In addition, the results from some of these studies are briefly discussed in chronological order.

Table 7.2 Quantitative Stress Measurements for DLC and Diamond Films

Film Stress (Pa) (C) = Compressive (T) = Tensile	Film Composition	Deposition Process	Reference
5. to 7 × 10^9 (C)	DLC on glass	Glow discharge	[19]
5 × 10^8 (C)	DLC on glass	e-beam heated carbon rod	[20]
7.5 × 10^8 (C) to 9.6 × 10^8 (T)	DLC on glass	Bias sputtered and plasma deposited	[21]
3. to 4 × 10^9 (C)	DLC on quartz glass and Si	Ion source	[22]
0.5 to 3. × 10^9 (C)	DLC on Si	Ion source	[23, 24]
1.6 × 10^9 (C)	DLC on glass	RF magnetron sputtering	[25]
≈ 10^9 (C)	DLC on ZnS and ZnSe	Ion source	[26]
1.2 × 10^9 (C)	DLC on Si	DC plasma reactor	[27]
9.4 to 139. × 10^6 (T)	Diamond on Si	Microwave plasma	[28]
2.1 to 4.7 × 10^9 (C)	Diamond on Si(100)	filament	[29, 30]

Stress measurements have been described by Enke [19] for diamond-like films on 0.15 mm (0.0059 inch) thick glass substrates. For DLC films, typical stresses were 5 to 7 × 10^9 Pa. Less stress was observed as the films became more graphitic which was attributed to the incorporation of less hydrogen in those films. Enke mentions that in the literature, stress is only observed for carbon coating processes involving hydrocarbons.

Low-stress films have been prepared by Zelez [21]. The low stresses were attributed to the low concentration of hydrogen in the bulk. Substrates used were Si, SiO_2, glass, Al, Al_2O_3, KBr, ZnMn ferrite, NaCl, stainless steel, various plastics, and paper. Stress was measured by beam-bending techniques on a thin glass disc and could be varied from compressive to tensile.

Gille and Rau [22] analyzed the buckling of carbon films on a glass substrate to derive the internal stress. They tried to improve upon the analysis of Matuda *et al.* [20] from which a somewhat smaller stress was derived (**Table 7.2**).

D. Nir [23, 24, 31] examines the stress for DLC coatings on silicon and various steels prepared by a DC glow discharge source. Several effects were analyzed. First, the stress increased for ion energies above 80 eV. Secondly, the stress did not appear to be related to the hydrogen content of the film which contradicts previous assumptions made, for example, by Enke [19], Zelez [21], and Anttila and coworkers [32]. Finally, changing from CH_4 to C_4H_{10} resulted in increased stress in the films which he speculated was due to larger molecular fragments not being easily accommodated on the surface.

Berry *et al.* [28] examined diamond films on a silicon substrate which had the unusual property of being under tensile stress. The films were grown at 1123 K and were 2 μm thick. The stress was measured as a function of temperature up to 700 K. The stress increased at low temperature but then leveled at higher temperatures. The results were attributed to the differential thermal expansion of diamond and silicon.

Specht and coworkers [29, 30] examined the strain in diamond films using X-ray diffraction. Three different types of diamond film morphologies were characterized which were labeled: microscrystalline, {111}, and {100}. The lattice constants of the various materials were the same as that of pure diamond. Therefore, the strains in the films were not due to expansion or contraction of the lattice (such as due to incorporation of impurities including hydrogen), but were likely created between grains due to interaction with the substrate. The strains measured were 2.4 to 5.2×10^{-3}. Assuming a modulus of 9.1×10^{11} Pa, a stress of 2.1 to 4.7×10^{9} Pa is calculated.

Ager and coworkers [33] considered whether the shifting and broadening of the Raman line from diamond films is due to stress. They observed that the diamond Raman line is shifted by 2.5 cm^{-1} to higher frequency which could be explained by a stress of 9.0×10^{8} Pa, which is consistent with other measurements in table 7.2. The Raman line is also wider than pure diamond which the authors speculated was due to varying degrees of strain in different crystallites. This explanation is not consistent with the X-ray analysis of Specht and coworkers [29, 30], however.

7.3 Measurements of Stress in DLC Films

Stress in the DLC coatings can cause deformation of a thin substrate. The stress in DLC coatings deposited at Sandia were determined from the deflection it caused in a thin aluminum substrate using the analysis of Stoney [34]. With this technique, the position of a thin substrate is measured before and after a DLC coating is applied and the stress determined from the deflection and mechanical properties of the substrate.

In order to observe a significant deflection of the sample, the DLC was deposited onto a thin aluminum substrate with a thickness of approximately 0.005 inches. The depositions were performed in the LAMPE reactor. The samples were laser or e-beam cut and were 0.25 x 2.25 inches. The laser or e-beam cutting was necessary to avoid crimping of the thin sample which occurred when a sheet metal cutter was used. The average thickness of the sample was determined by weighing the sample with a microbalance with a sensitivity of 0.00001 g and assuming a density for aluminum of 2.6989 g cm^{-3}.

A schematic for the apparatus to measure the elastic modulus and deflection is shown in **Fig. 7.1.** Before coating with DLC, the thin sample is rigidly clamped between two blocks which suspends the free end of the sample above a proximity detector. The two blocks holding the sample is mounted on a micrometer-driven platform (not shown) so that the sample can be moved a measured distance.

The elastic modulus of the thin sample must be known to calculate the stress in the DLC coating. This was measured by putting known weights on the free end of the sample and measuring the deflection of the sample using the proximity detector. Because the proximity detector does not have a perfectly linear response to position, the weights were applied to the sample, and then the micrometer was adjusted until the original proximity detector reading was achieved. The deflection of the sample caused by the weight was then determined directly from the change in the

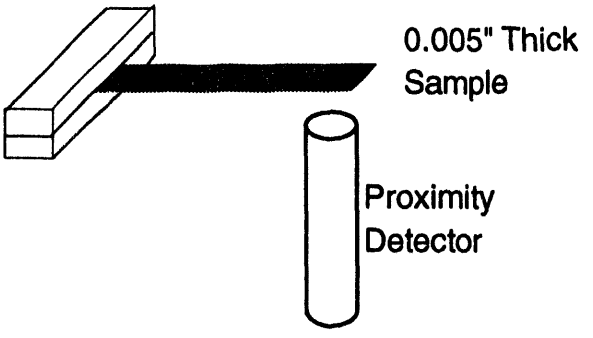

Figure 7.1. Schematic of Stress measuring apparatus.

micrometer readings. This procedure was repeated for weights of 10, 20, 50, 100, 200, 300, and 400 mg. A plot was made of deflection versus mass and the slope used in the formula for the elastic modulus determination. The elastic modulus was derived using the formula

$$E_s = \frac{4l^3 G}{w_s^3 \delta}$$

where E_s is the elastic modulus of the substrate, l is the length of the beam, w is the width of the beam,G is the weight on the end of the beam and δ is the deflection of the end of the beam [12]. G/δ is determined from the slope of the weight versus deflection plot.

Following measurement of the elastic modulus of the thin beam and initial position of the end of the beam, the sample and the two mounting blocks were then put into the deposition chamber and DLC deposited on the top side of the sample. The sample and two mounting blocks were then repositioned back onto the deflection measuring apparatus. The reproducibility of the mounting arrangement was ± 0.0002 inches. The deflection of the free end was then determined by moving the micrometer until the original proximity detector reading was obtained and the deflection of the sample determined from the change in micrometer readings. In order to calculate the stress in the coatings, the thickness of the coating was also needed which was measured using a profilometer. The stress is then calculated from

$$\sigma = \frac{E_s d_s^2 \delta^2}{3l^2 d_f}$$

where σ is the stress in the DLC coating, d_s is the thickness of the beam, and d_f is the DLC coating thickness [12].

Table 7.3 shows the results of stress measurements for DLC films deposited on an aluminum substrate using the plasma enhanced chemical vapor deposition system at Sandia. Only compressive stresses were measured in the films. The stress values in **Table 7.3** are all large, 2 to 4 GPa, but are consistent with stresses reported previously for DLC (**Table 7.2**). The results are also illustrated in **Figs. 7.2** and **7.3.**

Table 7.3 Measurements of Stress in DLC Coatings Prepared at Sandia

Sampling Number	Coating Depth (Å)	Deposition Time (min.)	Deposition Pressure (mTorr)	Stress (GPa)	Modulus (GPa)
DO021893.w1	1180	30	15.3	4.17	71.92
DO021993.w1	3753	60	15.3	3.41	81.93
DO022493.w1	7080	90	15.3	2.22	83.78

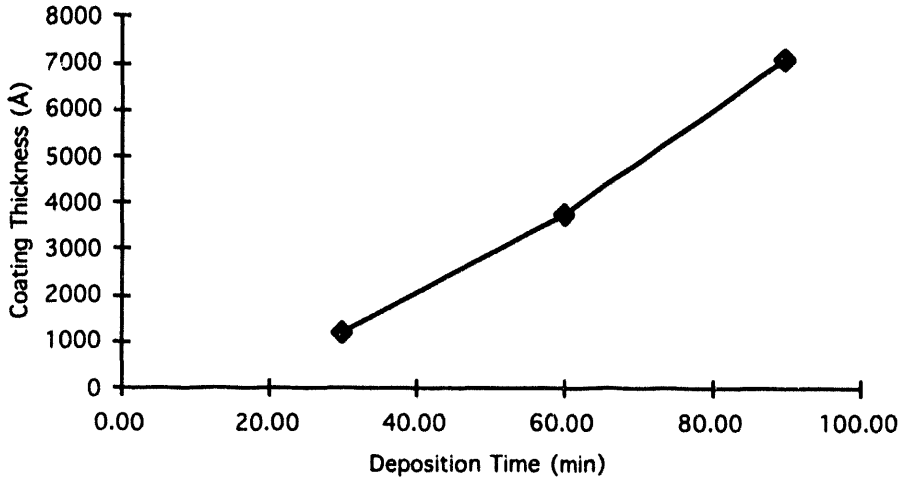

Figure 7.2. DLC coating thickness versus deposition time.

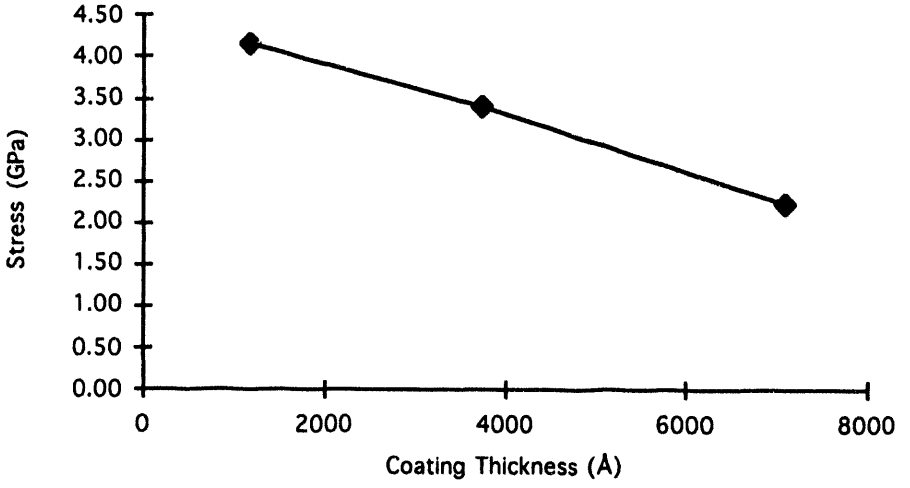

Figure 7.3. Stress versus coating thickness for DLC on aluminum substrates.

From the profilometer measurement, the deposition is nearly linear with deposition time, although there is an induction period for the deposition (**Fig. 7.2**). (Note, the deposition rate is more linear in the newer PECVD system (see section 2) than in the LAMPE system, because of improved process control in the PECVD system.)

The stress in the films, however, does not increase linearly with coating thickness. Instead, the stress is concentrated near the substrate interface. The measurements show that the stress is largest for the thinnest films and then decreases with time. This type of behavior has been reported for other thin films such as Ag, Cu, Sb, ZnS, and LiF [9]. This result is because this type of measurement yields only the average stress of the film. It has been demonstrated in these other systems, however, that the stress is not distributed uniformly throughout the films. Instead, the stress is concentrated in a region within 1000 Å of the substrate. Thus, as the average stress of thicker films is measured, it decays. It cannot be expected that the stress in DLC coatings should vanish at thick coverages, however. Instead, films of DLC above approximately 1.0 μm typically delaminate from substrates and the conventional explanation is that the total film stress overcomes the adhesive bonds of DLC to the substrate.

Initially, in these studies it was planned to perform in-situ measurements of stress during DLC film growth using interferometry. A problem was encountered, however, during the plasma growth of DLC, because of the self-electrical-bias of approximately 600 volts that the sample experiences as a result of the plasma. This bias caused an electrostatic deflection of the thin, flexible, sample away from its holder. This deflection was much larger than stress induced deflections. Thus the concept of in-situ stress measurements based upon deflection of a thin substrate was not feasible for our sample configuration.

8.0 Adhesion of DLC Coatings - Duane Outka

8.1 Mechanical and Chemical Properties of Diamond Relevant to Adhesion

DLC (diamond-like carbon) films possess a unique combination of properties including extreme hardness, chemical inertness, optical transparency, and electrical insulation. These films have therefore been proposed as protective coatings for a variety of technological devices including magnetic storage media, machine tools, and optical elements [35]. One difficulty in the application of DLC coatings has been obtaining good adhesion of the DLC coating to various substrates. This report reviews the subject of adhesion with respect to DLC and diamond coatings including a discussion of the mechanical and chemical properties of diamond relevant to adhesion; a review of previous studies of DLC film adhesion; and strategies for improving the adhesion of DLC coatings. Stress in DLC coatings is also important in adhesion and is discussed in the previous section.

8.1.1 Bulk Properties

Adhesion between two surfaces depends upon both mechanical and chemical interaction at the interface. Since DLC films are of interest largely for their similarity to diamond, it is useful to

first consider some of the bulk properties of diamond which are related to adhesion. The following analysis tries to put the adhesive strengths in perspective with more common chemical bonding and Van der Waals attractions.

Adhesion is partly due to physical or chemical bonding across an interface. To understand the relationship between bonding and adhesion, the strength of bonds within DLC itself are examined first. This is of interest because the adhesion strength of a DLC film can be no greater than the intrinsic strength of the DLC film itself (the internal strength of a material is called the cohesive strength). Since it is difficult to measure the properties of DLC, it is assumed that the properties of a DLC film are the same as bulk diamond. This approximation overestimates the strength of DLC, however. Diamond is held together by C-C bonds which have a bond energy of roughly 85 kcal mol^{-1}. The theoretical fracture energy of diamond can be calculated based on the number of bonds that must be broken in a particular direction. For example, the weakest cleavage plane for single crystal diamond is the (111) plane which has a theoretical surface fracture energy, γ, of 5.0 J m^{-2} [17]. The cohesive strength of diamond, σ_{th}, can be estimated by the formula

$$\sigma_{th} = \sqrt{\frac{E\gamma}{a}} \tag{1}$$

to be 1.9×10^{11} Pa where E is the elastic modulus and a is the nearest neighbor distance. This is the strength of diamond if it were determined solely by covalent bonding. As shall be seen, such bonding is much greater than typical bonding involved in adhesion of a coating.

At the other extreme, Van der Waal attraction between two ideal surfaces with attractions of approximately 10 kcal mol^{-1} results in a calculated adhesion strength of about 10^8 Pa [36]. Even though Van der Waal's bonding is usually considered weak, this type of attraction between two surfaces is large compared to typical adhesion strengths for coatings. For comparison, the upper limit for adhesion measurements using a commercially available Sebastion pull tester is only 4.5 to 6.9×10^7 Pa which is limited by the strength of an epoxy bond.

In real materials, however, the cohesive strength is limited not by the strength of the bonds but by the mechanical properties of the solid (i.e. cracks and fracture properties). For example, the actual tensile strength of diamond is measured to be 2.8×10^9 Pa which is two orders of magnitude smaller than the theoretical cohesive strength calculated above [17]. The tensile strength of most other materials is $< 1. \times 10^9$ Pa. To the extent that DLC shares this high tensile strength, the adhesion between a DLC film and a substrate will likely fail either in the interface region or in the substrate.

8.1.2 Interface Chemical Bonding

So far, the discussion of adhesion strength has considered only the bonding and mechanical properties of the DLC film or the substrate alone. The real issue for adhesion, however, is the

strength of the interface between the substrate and the DLC film. This is determined in part by the strength of bonding between substrate and film.

Very little is known about the bonding between DLC films and various substrates. Thus the bonding between a DLC film and a substrate can only be inferred from general chemical principles. For example, it might be expected that the strength of bonds at the DLC-substrate interface are related to the strength of substrate-carbon bonds in other compounds. Unfortunately, few measurements of bond dissociation energies involving metal-carbon bonds have been performed. A few bond dissociation energies are shown in **Table 8.1.** Most of the data concerns Group IIIb, IVb, and Vb elements to which relatively strong bonds are formed (40 to 90 kcal mol^{-1}). The little information regarding alkyl bonds to transition elements (Co and W) indicate they are somewhat weaker (18 to 38 kcal mol^{-1}).

Table 8.1 Carbon Bond Dissociation Energies

Bond	Bond Dissociation Energy (kcal mol^{-1})	Reference
$CH_2CHCH_2—Si(CH_3)_3$	70	[37]
$s\text{-}C_4H_9—Si(CH_3)_3$	90	[37]
$CH_3—ZnCH_3$	68	[37]
$C_2H_5—ZnC_2H_5$	57	[37]
$CH_3—Ga(CH_3)_2$	63	[37]
$C_2H_5—Ga(C_2H_5)_2$	50	[37]
$CH_3—Ge(CH_3)_3$	83	[37]
$CH_3—As(CH_3)_2$	67	[37]
$CH_3—CdCH_3$	60	[37]
$CH_3—In(CH_3)_2$	49	[37]
$CH_3—Sn(CH_3)_3$	71	[37]
$C_2H_5—Sn(C_2H_5)_3$	63	[37]
$CH_3—Sb(CH_3)_2$	61	[37]
$C_2H_5—Sb(C_2H_5)_2$	58	[37]
$CH_3—Tl(CH_3)_2$	40	[37]
$CH_3—Pb(CH_3)_3$	57	[37]
$C_2H_5—Pb(C_2H_5)_3$	55	[37]
$CH_3—Bi(CH_3)_2$	52	[37]
$CH_3—W(CH_3)_3$	38 (estimate)	[38]
Co-alkyl	18-25 (estimate)	[38]

Table 8.1 represents only one type of carbon bonding (i.e. metal-alkyl). There are many elements, however, which are not represented in Table 8.1 which form stable carbides using a different form of bonding and which is another prototype for the bonding between a DLC film and a substrate. The strength of such bonding is approximated by their thermodynamic properties which are shown in **Table 8.2.**

Table 8.2 Thermodynamic Properties of Carbides

Compound	ΔH^0_f (25 °C) (kcal mol^{-1})	ΔG^0_f (25 °C) (kcal mol^{-1})	Linear Coeff. of Thermal Expansion (at 25 °C) x 10^{-6} °C^{-1}
Al_4C_3	-30.9 [39]	-29.0 [39]	
CoC_3	9.5 [39]	7.1 [39]	
Cr_3C_2	-21 [39]	-21.2 [39]	8.0 [41]
	-9. to -29. [40]	-11. to -31 [40]	
Fe_3C	5.0 [39]	3.5 [39]	
MoC	34.4 [41]		5.95 [41]
Mo_3C_2	-14. [42]	-14.1 [42]	
Mo_2C	-11.5 [42]	-12.5 [42]	5.48 [41]
			7.8 to 9.3 [14]
Ni_3C	11.0 [39]		
SiC	-16.5 [42]	-15.9 [42]	4.63 [41]
TaC	-34.6 [42]	-34.6 [42]	8.2 [41]
	-32.3 to -53. [40]	-35. to -56. [40]	7.1 [14]
Ta_2C	-47. [42]	-47. [42]	
TiC	-43.8 [42]	-43.8 [42]	6.52 [41]
	-44.1 [40]	-45.8 [40]	8.0 to 8.6 [14]
UC	-21.1 [40]		9.47 [41]
UC_2	21 to 23 [40]		6.32 [41]
U_2C_3	-54. [39]		6.26 [41]
	-49. [40]		
WC	-9.09 [39]	-8.5 [42]	4.9 [41]
	-8.4 [42]		3.8 to 3.9 [14]
W_2C	-6.3 to -9.7 [40]		

The results in **Table 8.2** are summarized in **Table 8.3** which presents a portion of the periodic table showing which elements form stable carbides and which form unstable carbides. Two types of elements form stable carbides according to the free energies of formation in **Table 8.2.** These are the early transition elements such as Ti and Mo which form interstitial carbides and elements such as Si which forms covalent carbides. Substrates of these elements might therefore be expected to form strong adhesive bonds to DLC films. The late transition elements such as Ni, Cu, and Fe, in contrast, either have positive free energies for carbide formation or do not form stable carbides at all. Substrates of these elements might therefore be expected to form weak adhesive bonds to DLC films.

Table 8.3 Elements with Stable and Unstable Carbides

Be											B	C
Mg											Al	Si
Ca		Ti	V	Cr		~~Fe~~	~~Co~~	~~Ni~~	~~Cu~~	~~Zn~~	~~Zn~~	Ge
		Zr	Nb	Mo			~~Rh~~	~~Pd~~	~~Ag~~	~~Cd~~		
Ba		Hf	Ta	W				~~Pt~~	~~Au~~	~~Hg~~		~~Pb~~

Stable carbide
~~Unstable carbide~~

8.2 Previous Studies of DLC Film Adhesion

8.2.1 Quantitative Adhesion Studies

The preparation and properties of DLC films have been reviewed by Angus [6] and Tsai and Bogy [18] who briefly discuss the issue of adhesion. Angus *et al.* suggest that the best adhesion is obtained on substrates that form carbides such as Si, Fe, Ge, and Ti. Few quantitative measurements of adhesion of DLC films have been reported. Instead, adhesion is usually simply rated as either good or poor. To a large extent, this is a result of the difficulties of measuring adhesion for DLC films.

Table 8.4 list four studies where quantitative measurements of the adhesion strength have been reported. In two cases, the adhesion **energy** is reported which is converted to an approximate adhesion **strength** by dividing by the approximate interatomic separation, 1×10^{-10} m. The first two studies are based upon analysis of the buckling of DLC films on glass substrates. Matuda's [20] early measurement yielded an adhesion strength of approximately 10^9 Pa. Gille [22] in later work criticized the early analysis, however, and suggested that this was an order of magnitude too small. It is puzzling, however, that Gille calculates relatively large adhesion strengths based upon films which actually exhibit severe buckling and thus are poorly adherent. Gille also estimated the elastic modulus of the films to be 1.2 to 1.6×10^{11} Pa which is almost an order or magnitude smaller than bulk diamond (see **Table 7.1**). Mirtich [43] measures a lower limit for the adhesion strength of DLC on a ZnS and ZnSe substrate of 2. to 2.8×10^7 because failure occurred in the substrate. Kinbara and Baba try to deduce adhesive strengths from a scratch test which requires a number of assumptions. The last entries in **Table 8.4** provide comparisons to put the measured adhesion strengths in perspective.

Table 8.4 Quantitative Adhesion Measurements for DLC and Diamond Films

Adhesion Strength (Pa)	Type of Film Process	Deposition	Measurement Technique	Ref.
≈ 1 to 3×10^9 (0.1 to 0.3 J m^{-2})	DLC on glass	e-beam heated carbon rod	Film buckling analysis	[20]
≈ 4 to 7×10^{10} (4 to 7 J m^{-2})	DLC on glass	Electron and ion beam source	Film buckling analysis	[22]
$> 2.$ to 2.8×10^7 (failure occurred in substrate)	DLC on ZnS ZnSe with 200 to 1000 Å Ge or Si interlayer.	Ion source	Sebastion pull test	[43, 44]
2×10^9	DLC on glass	RF magnetron sputtering	Scratch test	[25]
$\leq 10^9$	Tensile strengths of most materials			
4.5 to 6.9×10^7	Epoxy strength in pull test			

8.2.2 Qualitative Adhesion Studies

More frequently, the adhesion of a DLC film is reported only in a qualitative manner (i.e., the film adhered or it did not) [19-27, 31, 32, 43-57]. It is difficult to compare the results from these various papers, because the deposition conditions, substrates, and techniques for evaluation of the coatings varied widely. Nevertheless, many of these papers have interesting insights regarding the adherence of DLC. Some of the more interesting results are summarized below.

D. Nir [23, 24, 31] briefly mentions that good DLC coatings can be obtained on silicon and various steels using a DC glow discharge source. He reports that adherence was improved by increasing the accelerating voltage.

Mirtich *et al.* [43, 44] made quantitative measurements of the adhesion of DLC on ZnS and ZnSe which were discussed above. Initially the adherence was poor (less than 2.8×10^5 Pa) and spalled almost immediately after deposit. Adhesion was not improved by (1) ion beam cleaning of the substrates prior to deposition or (2) various ion implantation techniques. Adhesion was improved by a thin, 0.02 to 0.1 μm, interlayer coating of Ge or Si such that failure occurred in the substrate rather than the interface during a pull test. Ge was better than Si as an interlayer because the latter failed with time. The DLC coatings were 0.1 μm thick and deposited using an ion source.

Anttila and coworkers [32] compared the adhesion of DLC films prepared by ion beams of C^+, CH_3^+, CH_4^+, and $C_2H_2^+$ on WC-Co substrates. Qualitatively, the hydrogen-containing beams exhibited poor adherence whereas the C^+ beams exhibited good adherence suggesting the hydrogen incorporation in the solid had an adverse effect on adhesion.

Grill and coworkers [48] used Si interlayers to improve the adhesion of DLC films to Co, Cr, and their alloys. The samples consisted of a Si wafer backing–metal–Si interlayer–DLC. The optimal thickness of the Si interlayer for adhesion was 0.01 μm. The adhesion was qualitatively tested with a Sebastion pull tester and failure occurred in the silicon wafer which backed the metal substrate.

Wittmer *et al.* [51] have examined the adhesion of DLC films on a Ge(100) surface. Ge does not form a carbide so strong adherence is not expected. DLC films in this paper using an ion source were adherent, however, which is attributed to atomic intermixing and the formation of a metastable as deduced from chemical shifts in XPS.

Moazed and coworkers [53] examined the contact between diamond films and various metals to evaluate the resistivity of electrical contacts. Good electrical contacts were made by sputter depositing various contacts including nickel, titanium/gold, titanium/platinum, molybdenum, molybdenum/gold, molybdenum/nickel/gold, and tantalum/gold. Film thicknesses were 10 to 50 nm. Adherence of these contacts to the diamond was attributed to the formation of a carbide layer which required an annealing step between 750 and 1100 C.

Galuska [56] considers the bonding of a copper film to a glassy carbon substrate. This is a difficult adhesion problem because copper and carbon do not react to form any known stable carbon compounds. Implanted aluminum atoms were chosen to try to improve adhesion because of the exothermic Al-Cu (Cu_2Al: ΔH^0_f = -69.0 kJ mol^{-1} at 25 °C) and Al-C (Al_4C_3: ΔH^0_f = -208.8 kJ mol^{-1} at 25 °C) reactions. A scratch test was used to show that the Al improved adhesion. XPS and AES analysis suggest the increased adhesion was due to Cu-Al-C bonding.

Wang and coworkers [57] improved the adhesion of DLC films on Si using metal interlayers. The films were deposited using a RF microwave plasma. Both Ti and Ta improved adhesion up to metal concentrations of 45 and 12 atom percent, respectively. Adhesion was qualitatively evaluated using a scratch test.

8.3 Strategies to Improve Adhesion of DLC Coatings

8.3.1 Remove Contaminants

The first and most obvious strategy to improve adhesion is to remove contaminants from the surface of the substrate prior to deposition. Many papers have mentioned the importance of cleaning for good adhesion [19, 26, 52]. This can be accomplished by degreasing of the substrate before deposition and by sputtering before deposition using the plasma.

8.3.2 Mechanical Interlocking

Second, another obvious strategy to improve adhesion is to provide mechanical interlocking of substrate and film. This is not considered in detail in the literature but could be accomplished by scratching, or patterning of the substrate.

8.3.3 Interlayer

Several different types of interlayer materials have been shown to improve the adhesion between a substrate and a DLC film. Ge and Si have been used to improve adhesion of DLC to ZnS and ZnSe [43, 44]. Si has been used to improve the adhesion of DLC to Co, Cr, and their alloys [48]. Al has been used to improve the adhesion of DLC to copper [56]. BN and SiC have been used to improve diamond adhesion and nucleation on ZnS and Si [58]. Ti and Ta have been used to improve the adhesion of DLC on Si [57].

The role of such interlayers so far has been to improve the chemical bonding between the substrate and DLC. This could be important for substrates such as copper with which carbon does not easily react. Likely interlayer materials are those elements in **Table 8.2** which form carbides with large free energies of formation. In several studies chemical shifts have been observed in XPS and AES which indicate that the interlayers do react with the DLC. For example, Si interlayers react with DLC to form SiC [54]; Ge interlayers react with DLC [51]; and Al interlayers react with both Cu substrates and DLC [56].

Interlayers could also improve adhesion by reducing stress in the film. This could be the result of changing the morphology of the deposit and thus reducing the intrinsic stress of the film or by providing a graded interlayer between the substrate and DLC to match their mechanical and thermal properties. These issues have not been considered in detail for DLC films but are considered by Murakawa and Watanabe [59] for the case of BN films on Si.

8.3.4 Reduce Stress and Optimize Process Parameters

Finally, process parameters could be varied to try to minimize the stress and improve the adhesion of DLC films. Parameters which could be changed include substrate temperature, deposition rate, and residual gas composition. These could have an affect on the intrinsic stress in the film by changing the morphology of the deposit. At this point, however, it is not understood at a microscopic level how the deposition process parameters affect the characteristics and adhesion of DLC films.

Several papers have indicated that process parameters do affect the characteristics of DLC films. For example, Nir [23, 24, 31] examined the stress for DLC coatings on silicon and various steels prepared by a DC glow discharge source. He observed that stress increased for ion energies above 80 eV. He also found that changing from CH_4 to C_4H_{10} resulted in increased stress in the films. Ion energy is also implicated in the work by Ham and Lou [27] who describe the deposition of DLC films on a variety of substrates using a DC plasma reactor. Good adhesion was obtained with most materials except for Au, Cu, W, or stainless steel containing Cu. It was postulated that the poor adhesion was due to sputtering of the soft substrate materials. Anttila and coworkers [32] found that films with high hydrogen contents had poor adhesion. They investigated heating the substrate up to 400 °C which resulted in only a slight decrease in hydrogen content.

The effect of process parameters on DLC film deposition has also been considered in the review by Tsai and Bogy [18]. They offer several suggestions. (1) Ion bombardment during deposition may create high compressive stresses by "peening" the surface. (2) For some systems, there

appears to be a correlation between hydrogen content and compressive stress. The highest stresses are observed for films in the diamond-like properties region (high hydrogen content) and decrease toward the graphite-like region. (3) Background gases during deposition may affect adhesion. For example, it has also been reported that wrinkling does not occur for even thick films under vacuum, but does occur upon exposure to a gas (which gas is not important). This suggests that gas atoms diffuse into the interface between the coating and the substrate leading to failure of adhesion of the film to the substrate and leading to wrinkles. The effect of background gases has been examined in other systems by Abermann and coworkers [60, 61] who studied Al, Cr, and Fe film formation under UHV conditions. They found that O_2 and H_2O background gases could change the stress in films by changing the morphology of the deposit and the bonding of the film to the substrate.

8.4 Chemical Issues for Interlayers Used to Improve the Adhesion of Carbon Films on Iron Substrates

Earlier, the chemical basis for DLC and diamond film adhesion by tabulating the strength of carbon bonding to various other elements. This was of interest in (1) predicting which substrates would exhibit good adhesion to DLC overlayers and (2) suggesting which elements could be used as interlayers to promote the adhesion of carbon films on various substrates. The interlayer analysis was incomplete, however, because it only considered the bonding of the interlayer to the carbon overlayer. It did not consider the bonding of the interlayer to the substrate, because there were too many possible combinations of substrates and interlayers. Iron and iron alloys are of special interest because of the importance of stainless steels. This section, therefore, considers the chemical basis for improving the adhesion of carbon films to iron substrates.

The enthalpy of formation of iron carbide, Fe_3C, is +5 kcal mol^{-1} which indicates that the bonding of carbon to iron is relatively poor. This suggests that the direct adhesion of carbon films to an iron substrates would be poor. This is consistent with the results shown in section 5.2 above. One strategy for improving the adherence of DLC films to iron is to use an interlayer which bonds well to both iron and carbon. This section examines the thermodynamics of various possible combinations in order to suggest good candidates for the interlayer.

The chemistry of iron is similar to that of carbon compounds in the sense that iron not only forms compounds but also forms solid solutions with various elements. **Table 8.5** summarizes the behavior of iron in forming binary alloys and compounds [62]. From this table it is seem that iron forms compounds with the early transition elements such as Ti and W as well as most elements of Group III (Boron column) and those to the right. Iron forms solid solutions with the mid-transition elements such as Co, Pd and Ir. Iron does not react with some elements such as the alkali metals (Li column), the alkaline earth elements (Mg column), certain heavy metals (e.g. Hg and Tl), and the noble gases.

Table 8.5 Binary Alloys and Compounds of Iron [62]

H part sol.																	**He**
Li Im	**Be** 3C											**B** 3C	**C** 4C+	**N** 3C+	**O** 3C	**F** 3C	**Ne**
Na Im	**Mg** Im											**Al** 5C	**Si** 4C	**P** 4C+	**S** 4C+	**Cl** 2C	**Ar**
K Im	**Ca** Im	**Sc** 2C	**Ti** 3C	**V** SS	**Cr** SS	**Mn** SS	**Fe**	**Co** SS	**Ni** SS	**Cu**	**Zn** 3C	**Ga** 5C	**Ge** 4C	**As** 3C+	**Se** 2C	**Br** 2C	**Kr** part. sol.
Rb Im	**Sr** Pr. Im	**Y** 4C	**Zr** 1C	**Nb** 3C	**Mo** 2C	**Tc** 1C	**Ru**	**Rh** 1C+	**Pd** SS	**Ag** Im	**Cd** Pr. Im	**In**	**Sn** Im	**Sb** 2C	**Te** 4C	**I** 3C	**Xe**
Cs Im	**Ba** Im	**La**	**Hf** 1C	**Ta** 1C	**W** 2C	**Re** 3C	**Os**	**Ir** SS	**Pt** SS	**Au**	**Hg** Im	**Tl** Im	**Pb** Im	**Bi** Im	**Po**	**At**	**Rn** part. sol.

Abbreviations

SS	Solid Solution
Im	Immiscible
Pr. Im	Probably Immiscible
C	Compounds
part. sol.	Partially Soluble

While a variety of iron compounds and alloys have been identified, few standard thermodynamic values have been measured for them. A list of the enthalpies of formation for several binary iron compounds and alloys which are known at room temperature are shown in **Table 8.6.** From **Table 8.6** is it seen that iron forms alloys with most metals with small negative heats of formation.

Table 8.6 Thermodynamic Properties of Binary Iron Compounds and Alloys

Compound	ΔH^0_f (25 °C) (kcal mol^{-1})	References
Al-Fe alloys	-3.8 to -6.7	[63]
Fe-Si alloys	-5.6 to -9.6	[64]
$FeSb_2$	-3.6	[64]
FeTi	-4.9	[64]
Fe_2U	-2.6	[64]
Co-Fe alloys	-2.3	[64]
Cr-Fe alloys	+1.1 to +1.5	[64]
Fe-Mn alloys	-1.2	[64]
Fe-Ni alloys	-1.0	[64]

In many cases, thermodynamic values for iron alloys (i.e. solid solutions) have been measured at elevated temperature as shown in **Table 8.7.** Although it is difficult to use such high temperature results to directly predict room temperature adhesive behavior, a few generalizations can be made about the behavior of iron in forming alloys. In principle, the heat of formation at room temperature could be calculated from the heat of reaction at elevated temperature, T_2, using

$$\Delta H^0_{rxn}(T_2) = \Delta H^0_f(25^\circ C) + \int_{25\,^\circ C}^{T2} [C_p(\text{Products}) - C_p(\text{Reactants})]\, dT$$

where C_p is the heat capacity. For most metals, however, the ΔH^0_{rxn} at elevated temperature for iron is small, less than 5 kcal mol^{-1} (**Table 8.7**). The major driving force for the formation of the alloy is the entropy of mixing. Thus the heats of formation at room temperature of many other elements are expected to be comparable to those in **Table 8.7** (i.e. less than 5 kcal mol^{-1}).

Table 8.7 Thermodynamic Properties of Binary Iron Compounds and Alloys at Elevated Temperature

Compound	ΔH^0_f (kcal mol^{-1})	Temperature (K)	References
Fe-Au alloys	+1.6	1123	[63]
Fe-Cu alloys	+2.1	1823	[63]
Fe-Mn alloys	-1.2	1450	[63]
Fe-Ni alloys	-1.1	1200	[63]
Fe-Pd alloys	-2.9	1273	[63]
Fe-Te alloys	-5.4	793	[63]
Fe-V alloys	+2.2	1600	[63]
Fe-Zn alloys	+0.5	1066	[63]
Fe-Zr alloys	-5.9	1023	[63]

The small heats of formation in **Tables 8.6** and **8.7** must be cautiously interpreted. In particular, such small values do not indicate that iron forms flimsy compounds with weak bonds. Instead, it must be remembered that the heat of formation is a relative value of the stability of a compound with respect to the constituent elements. If the elements themselves have strong internal bonding (i.e. large cohesive energies) then the bonding in the alloy can also be large despite a small heat of formation for the alloy. To understand this point, it is useful to consider a thermodynamic cycle involving the formation of an alloy (shown below). For example, consider the formation of a 1:1 Fe-Al alloy by direct reaction of the solid elements (rxn. 1 below); and by an alternative route involving sublimating Fe (rxn. 2), sublimating Al (rxn. 3), reacting gaseous Fe and Al (rxn. 4), and, finally, condensing gaseous FeAl (rxn. 5).

$$\begin{array}{ccccc} \text{Fe (s)} & + & \text{Al (s)} & \xrightarrow{(1)} & \text{FeAl (s)} \\ \downarrow (2) & & \downarrow (3) & & \downarrow (5) \\ \text{Fe (g)} & + & \text{Al (g)} & \xrightarrow{(4)} & \text{FeAl (g)} \end{array}$$

Reactions 1 through 5 can be identified as: (1) is the heat of formation of FeAl; (2) is the heat of sublimation of Fe; (3) is the heat of sublimation of Al; (4) is the heat of reaction between gaseous Al and Fe; and (5) is the heat of sublimation of FeAl. Since the starting and ending materials are the same, the following relation holds for the enthalpies of reactions 1 through 5:

$$\Delta H(1) = \Delta H(2) + \Delta H(3) + \Delta H(4) - \Delta H(5). \quad (1)$$

Note, that the cohesive energy of FeAl (s) which is the energy required to transform a compound into atoms, is by definition:

$$\Delta H(\text{cohes.}) = -(\Delta H(4) - \Delta H(5)). \quad (2)$$

The magnitude of this cohesive energy is a direct measure of the stability of the solid and a measure of the chemical contribution to the adhesive properties of this compound. Note also, that the cohesive energies of Fe and Al are simply $\Delta H(2)$ and $\Delta H(3)$, respectively. Rearrangement of eqs. (1) and (2) yields:

$$\Delta H(\text{cohes.}) = \Delta H(2) + \Delta H(3) - \Delta H(1). \quad (3)$$

The significance of eq. (3) is that the cohesive energy of FeAl depends not only upon the heat of formation of the compound, $-\Delta H(1)$, but is also directly related to the cohesive energies of Fe and Al, $\Delta H(2) + \Delta H(3)$. Thus, although the heat of formation of FeAl is small, approx. -7 kcal mol^{-1}, the cohesive energy of FeAl is large because the cohesive energies of Fe and Al individually are large. For example, the cohesive energy of Fe is 98.7 kcal mol^{-1} while that of Al is 78.1 kcal mol^{-1} [65]. These values are large and changes of 5 to 7 kcal mol^{-1} in forming the Fe-Al alloys are comparatively small. Thus the bonding of iron to a variety of elements as shown in Tables 2 and 3 is expected to be strong and comparable to the large cohesive bonding holding elemental iron together.

In conclusion, based upon chemical considerations, iron is expected to form strong bonds and thus exhibit good adhesion to a variety of elements. Although precise thermodynamic data is scanty, it can be argued that iron will form strong bonds to all of the elements in **Table 8.4** with which iron forms compounds or solid solutions. All of these elements are thus good candidates for interlayers for improving adhesion to iron substrates including the elements which were identified previously as forming good bonds with carbon. Thus the more restrictive issue for improving the adhesion of carbon films to iron substrates is the bonding of the interlayer to the carbon film. Interlayer materials which are recommended to improve adhesion are either (1) early transition elements such as Ti and Ta or (2) elements which form covalent carbides such as Si, Al, and B.

9.0 Hardness Testing - Duane Outka and Wen Hsu

The hardness and elastic modulus of a DLC film was measured using a nanoindenter. The sample was a 0.67 μm thick DLC coating on a Si(111) substrate. The deposition was performed in the LAMPE system and the sample number was 012093.W1. The nanoindentation results were supplied by Mitchell Trkula of Los Alamos National Laboratory. The analysis of nanoindentation data is described in the references [66, 67].

The results of 12 different indents were averaged to obtain a hardness of 29.1 ± 0.7 GPa and an elastic modulus of 230 ± 3 GPa. The indent sequence consisted of loading at a rate of 250 $\mu N\ s^{-1}$ to a depth of approximately 260 nm; holding for 25 sec to examine the creep; unloading at 300 $\mu N\ s^{-1}$ and holding for 100 seconds to examine the thermal drift. The results have been corrected for the tip function, and a value of 0.25 has been assumed for Poisson's ratio in calculating the elastic modulus.

The results indicate that the DLC has extreme mechanical properties, although not as large as those of crystalline diamond. For example, DLC has a measured hardness of 29.1 GPa. This is somewhat smaller than diamond which has a hardness of 55 to 112 GPa, but is larger than that of SiC (25.5 GPa), sapphire (21.6 GPa), and silicon (11.3 GPa) [68]. DLC also has a large elastic modulus of 230 GPa. This is smaller than that of crystalline diamond which is 910 GPa [14], but is still larger than many materials shown in **Table 7.1.**

10.0 Conclusions - Wen Hsu

We have developed a new plasma-based process for depositing DLC films. The main attraction of this process is its ability to conformally coat three dimensional objects. In contrast to other line-of-sight techniques, uniform coverage is accomplished without rotating the object to be coated or rastering the coating source. This simplification can be a major cost saving for large-scale manufacturing. Furthermore, the process is easily scaleable to coat large areas; it is conceivable to coat areas of 1 m^2. The uniformity of the discharge can be controlled to give uniform deposition.

The bulk of our effort on this project has focused on characterizing the films deposited using our plasma-enhanced CVD process and comparing them to properties of DLC films deposited using other techniques that have been reported in the literature. Our general finding is that our process produce films of equal quality—they are as hard, atomically smooth, lubricious, and chemically inert—as that produced by other processes. The DLC films can also be deposited on low temperature materials, such as plastics.

The whole technology of DLC films, however, can benefit from further research. We have identified two issues: First, virtually all reports, including our studies, show that DLC films have high levels of stress. This concurrence suggests that the level of stress is independent of the details of the deposition process. We speculate that the stress is a consequence of the high energetics of the particles that are prevalent in all deposition processes. In applications where films

of only a few microns are required, the stress will not pose problems. However, at greater thicknesses DLC films can peel off when the interface between the film and the substrate is compromised, such as by chemical attack or thermal cycling. We have not looked in detail at methods of overcoming this stress, but we speculate the introduction of impurity atoms into the lattice will be one technique for reducing the stress.

A second area that deserves further attention is the formation of pin-holes. Our work showed that microscopic pin-holes are present in the films. For applications that require chemical protection, the pin-holes limit the effectiveness of the protection. We have been able to reduce the number of pin-holes by using multi-layers of overcoatings, but they are not totally eliminated. This suggests that pin-holes are caused by a concentration of stress at surface imperfections. Thus reduction of stress could potentially reduce pin-holes as well. Both issues have hopeful directions to pursue.

These two problems do not limit the usefulness of DLC film for certain applications. For example, our process is used to coat stronglinks supported under the Product Application Team program. The requirements are to have low wear, low friction, low debris-generation, and a conformal coating. DLC coated parts are now being evaluated. Initial indications are that the wear, friction, adhesion, and thermal stability meet the required specifications. There has also been interest in DLC coatings from industry as a coating to reduce particulates in semiconductor manufacturing, and as a chemical-resistant and wear-resistant coating for mechanical seals. We also continue to actively search for further applications for DLC.

11.0 Acknowledgments

The authors wish to acknowledge the technical assistance of Dave Tung, Les Brown, Steve Bosson, John Weeks, and Josh Whaley in setting-up the PECVD reactor. We would also like to acknowledge the assistance of Andrew Gardea for polishing of aluminum disks for chemical resistance testing, of Ja Le Yio for chemical resistance testing, and of Chris Rood and Bernie Bernal for SEM analysis related to the chemical resistance testing.

12.0 References

1. S. Aisenberg and R. Chabot, J. Appl. Phys., 42 42 (1971).
2. L. Holland and S. M. Ojha, Thin Solid Films, 48 L15 (1978).
3. L. Holland and S. M. Ojha, Thin Solid Films, 58 107 (1979).
4. C. Weissmantel, K. Bewilogua, and C. Schurer, Thin Solid Films, 61 L1 (1979).
5. C. Weissmantel, *et al.*, Thin Solid Films, 96 31 (1982).
6. J. C. Angus, P. Koidl, and S. Domitz, "Carbon thin films," in *Plasma Deposited Thin Films*, J. Mort and F. Jansen, Editor (CRC Press, Inc., Boca Raton, Florida, 1986) p. 89.
7. W. L. Hsu, *et al.*, in *Plasma Processing and Synthesis of Materials*, D. Apelian and J. Szekely, Editor (Materials Research Society, Pittsburgh, PA, 1987) p. 155.
8. J. E. Field, *The Properties of Diamond.* (Academic, New York, 1979) 644.
9. R. W. Hoffman, "The mechanical properties of thin condensed films," in *Physics of Thin Films*, G. Hass and R.E. Thun, Editor (Academic, New York, 1966) p. 266.
10. K. L. Chopra, *Thin Film Phenomena.* (McGraw-Hill, New York, 1969) .
11. D. E. Gray, ed. *American Institute of Physics Handbook.* 3rd edition ed. (McGraw-Hill, New York, 1972)
12. D. S. Campbell, "Mechanical properties of thin films," in *Handbook of Thin Film Technology*, L.I. Maissel and R. Glang, Editor (McGraw-Hill, New York, 1970) p. 12.
13. R. C. Weast, ed. *Handbook of Chemistry and Physics.* 70th ed. (CRC Press, Boca Raton, Florida, 1989).
14. H. Holleck, J. Vac. Sci. Technol. A, 4 2661 (1986).
15. J. M. Gere and S. P. Timoshenko, *Mechanics of Materials.* 3rd ed. (PWS-Kent, Boston, 1990) .
16. R. J. Jaccodine and W. A. Schlegel, J. Appl. Phys., 37 2429 (1966).
17. J. E. Field, "Strength and fracture properties of diamond," in *The Properties of Diamond*, J.E. Field, Editor (Academic, New York, 1979) p. 281.
18. H.-c. Tsai and D. B. Bogy, J. Vac. Sci. Technol. A, 5 3287 (1987).
19. K. Enke, Thin Solid Films, 80 227 (1981).
20. N. Matuda, S. Baba, and A. Kinbara, Thin Solid Films, 81 301 (1981).

21. J. Zelez, J. Vac. Sci. Technol. A, 1 305 (1983).

22. G. Gille and B. Rau, Thin Solids Films, 120 109 (1984).

23. D. Nir, J. Vac. Sci. Technol. A, 4 2954 (1986).

24. D. Nir, Thin Solid Films, 146 27 (1987).

25. A. Kinbara and S. Baba, Thin Solid Films, 163 67 (1988).

26. J. T. Keeley and T. L. C. Wu, in *First international symposium on diamond and diamond-like films* (The Electrochemical Society, 1989) 250.

27. M. Ham and K. A. Lou, J. Vac. Sci. Technol. A, 8 2143 (1990).

28. B. S. Berry, *et al.*, Appl. Phys. Lett., 57 302 (1990).

29. E. D. Specht, R. E. Clausing, and L. Heatherly, J. Mater. Res., 5 2351 (1990).

30. R. E. Clausing, *et al.*, Carbon, 28 762 (1990).

31. D. Nir, Thin Solid Films, 112 41 (1984).

32. Anttila, *et al.*, Appl. Phys. Lett., 50 132 (1987).

33. J. W. Ager, D. K. Veirs, and G. M. Rosenblatt, Phys. Rev. B, 43 6491 (1991).

34. G. G. Stoney, Proc. Roy. Soc., 32 172 (1909).

35. K. E. Spear, J. Am. Ceram. Soc., 72 171 (1989).

36. T. Hull, J. S. Colligon, and A. E. Hill, Vacuum, 37 327 (1987).

37. R. C. Weast, ed. *Handbook of Chemistry and Physics.* 70th ed. (CRC Press, Boca Raton, Florida, 1989) F-206.

38. J. Halpern, Acc. Chem. Res., 15 238 (1982).

39. F. D. Rossini, *et al., Selected Values of Chemical Thermodynamic Properties, National Bureau of Standards Circular 500.* (U. S. Government Printing Office, Washington, DC, 1952).

40. E. K. Storms, *The Refractory Carbides.* (Academic, New York, 1967).

41. P. T. B. Shaffer, *Plenum Press Handbooks of High-Temperature Materials.* (Plenum, New York, 1964).

42. H. L. Schick, *Thermodynamics of Certain Refractory Compounds, Volume 2.* (Academic, New York, 1966).

43. M. J. Mirtich, *et al.*, J. Vac. Sci. Technol. A, 6 2680 (1986).

44. D. M. Swec, *et al.*, J. Vac. Sci. Technol. A, 4 3030 (1986).

45. K. Miyoshi and D. H. Buckley, Appl. Surf. Sci., 6 161 (1980).

46. K. Shibuki, *et al.*, Surf. Coat. Technol., 36 295 (1988).

47. K. Saijo, *et al.*, Surf. Coat. Technol., 43/44 30 (1990).

48. A. Grill, B. Meyerson, and V. Patel, J. Mater. Res., 3 214 (1988).

49. R. C. McCune, *et al., in Thin Films: Stresses and Mechanical Properties* (Materials Research Society, 1989) 261.

50. M. Murakawa and S. Takeuchi, Thin Solid Films, 181 443 (1989).

51. M. Wittmer, D. Ugolini, and P. Oelhaven, in *First international symposium on diamond and diamond-like films* (The Electrochemical Society, 1989) 353.

52. A. L. Lin, *et al.*, in *First international symposium on diamond and diamond-like films* (The Electrochemical Society, 1989) 261.

53. K. L. Moazed, *et al.*, in *First international symposium on diamond and diamond-like films* (The Electrochemical Society, 1989) 466.

54. K. G. Tschersich, in *First international symposium on diamond and diamond-like films* (The Electrochemical Society, 1989) 576.

55. C.-T. Kuo, T.-Y. Yen, and T.-H. Huang, J. Mater. Res., 5 2515 (1990).

56. A. A. Galuska, Surf. Coat. Technol., 43/44 975 (1990).

57. M. Wang, X. Jiang, and B. Stritzker, Thin Solid Films, 197 57 (1991).

58. T. Hartnett, *et al.*, J. Vac. Sci. Technol. A, 8 2129 (1990).

59. M. Murakawa and S. Watanabe, Surf. Coat. Technol., 43/44 145 (1990).

60. R. Abermann, Thin Solid Films, 188 385 (1990).

61. G. Thurner and R. Abermann, Thin Solid Films, 192 (1990).

62. K. P. Staudhammer and L. E. Murr, *Atlas of Binary Alloys.* (Marcel Dekker, Inc., New York, 1973) .

63. NBS, *Selected Values of the Thermodynamic Properties of Binary Alloys.* (American Society for Metals, Metals Park, OH, 1973) .

64. *Metals Reference Book.* 5th ed. ed. C.J.S. Ed. (Butterworths, Boston, 1976) .

65. C. Kittel, *Introduction to Solid State Physics.* sixth ed. (Wiley, New York, 1986) .

66. M. F. Doerner and W. D. Nix, J. Mater. Res., 1 601 (1986).

67. G. M. Pharr and W. C. Oliver, MRS Bulletin, 17 28 (1992).

68. C. A. Brookes, "Indentation Hardness," in *Properties of Diamond,* J.E. Field, Editor (Academic, New York, 1979) p. 383.

UNLIMITED RELEASE

INITIAL DISTRIBUTION:

MS 0320	Lopez, Laura, LDRD Office (Org. 1011)
MS 0336	Eagan, R. J. (Org. 1700)
MS 0340	Dugger, Mike (Org. 1832)
MS 0340	Salzbrenner, R. J. (Org. 1832)
MS 0342	Headley, Thomas J. (Org. 1822)
MS 0367	Peebles, Diane E. (Org. 1812)
MS 0469	Ives, Edwin E. (Org. 5200)
MS 0471	Callahan, M. W. (Org. 5092)
MS 0641	Gunckel, F. J. (Org. 2643)
MS 0641	Urenda, Ruben S. (Org. 2643)
MS 0641	Varga, K. S. (Org. 2643)
MS 9001	Crawford, John C. (Org. 8000)
MS 9005	Wright, James B. (Org. 5300)
MS 9043	Kee, Robert J. (Org. 8745)
MS 9052	Allendorf, Mark D. (Org. 8361)
MS 9052	Hardesty, Donald R. (Org. 8361)
MS 9054	McLean, William J. (Org. 8300)
MS 9102	Tung, Dave (Org. 8416)
MS 9103	McKelvey, Ed L. (Org. 8111)
MS 9161	McCarthy, Kevin (Org. 8342)
MS 9161	Stulen, Richard. H. (Org. 8342)
MS 9161	Wolfer, W. G. (Org. 8341)
MS 9162	Fox, Cairn (Org. 8347)
MS 9162	Hsu, Wen (Org. 8347) (10)
MS 9162	McMaster, Mark (Org. 8347)
MS 9162	Outka, Duane (Org. 8347) (10)
MS 9162	Pontau, Arthur (Org. 8347)
MS 9162	Weeks, John (Org. 8347)
MS 9162	Whaley, Josh (Org. 8347)
MS 9162	Phillips, Kristen (Org. 8347) (5)
MS 9162	Bosson, Steve (Org. 8347)
MS 9163	Wilson, K. L. (Org. 8304)
MS 9402	Brown, Les (Org. 8715)
MS 9402	Guthrie, Steven E. (Org. 8715)
MS 9402	Shepodd, Timothy J. (Org. 8711)
MS 9402	Thomas, George J. (Org. 8715)
MS 9402	Yang, Nancy (Org. 8715) (5)
MS 9402	Bernal, Bernie (Org. 8715)
MS 9402	Gardea, Andrew (Org. 8715)

MS 9402	Rood, Chris (Org. 8715)
MS 9404	Boehme, Dale (Org. 8713) (5)
MS 9404	Clift, Miles (Org. 8713)
MS 9404	Goods, Steven H. (Org. 8714)
MS 9404	Johnsen, Howard A. (Org. 8713)
MS 9404	Ottesen, David K. (Org. 8713) (5)
MS 9404	Wang, Jim C. F. (Org. 8713)
MS 9404	Yio, Ja Le (Org. 8713)
MS 9405	Lindner, Duane L. (Org. 8701)
MS 9022	Mail Distribution (8533-1) for OSTI (10)
MS 9022	Mail Distribution (Org. 8533-1)/Technical Library Processes, MS 0899, (Org. 7141)
MS 0899	Technical Library Processes Department (Org. 7141) (4)
MS 9018	Central Technical Files (Org. 8523-3) (3)

DATE
FILMED
6/14/94
END